# Changes in the distribution of Al and particulate Fe along A16N in the eastern North Atlantic Ocean between 2003 and 2013: Implications for changes in dust deposition

Pamela M. Barrett[a,b*], Joseph A. Resing[b], Nathaniel J. Buck[b], William M. Landing[c], Peter L. Morton[c], Rachel U. Shelley[c,1]

[a]School of Oceanography, University of Washington, Seattle, WA, USA
[b]Joint Institute for the Study of Atmosphere and Ocean, University of Washington PMEL/NOAA, Seattle, Washington, USA
[c]Department of Earth, Ocean, and Atmospheric Science, Florida State University, Tallahassee, Florida, USA
[1]Now at Laboratoire des Sciences de l'Environnement Marin, Institut Universitaire Européen de la Mer, Plouzané, France

*Corresponding author: Pacific Marine Environmental Laboratory, 7600 Sand Point Way NE, Seattle, WA 98115, USA. Tel.: +1 206 526 6452; fax: + 1 206 526 6054.

Email addresses: barrettp@uw.edu (P.M. Barrett), joseph.resing@noaa.gov (J.A. Resing), nathan.buck@noaa.gov (N.J. Buck), wlanding@fsu.edu (W.M. Landing), pmorton@fsu.edu (P.L. Morton), rachel.shelley@univ-brest.fr (R.U. Shelley)

**Abstract**

Particulate Al and Fe and dissolved Al concentrations were analyzed in seawater samples from the upper 1000 m of the eastern North Atlantic Ocean along the CLIVAR/$CO_2$ Repeat Hydrography program section A16N in summer 2013, repeating trace metal observations made along the A16N transect a decade earlier. Upper-ocean trace metal distributions in the equatorial and subtropical regions of the North Atlantic are heavily influenced by atmospheric aerosol sources. Using changes in the concentrations of subsurface particulate Al and Fe and mixed-layer dissolved Al in the equatorial North Atlantic, we estimate dust deposition to surface waters in the eastern North Atlantic increased by approximately 15% between 2003 and 2013. Increased concentrations of dissolved Al in subtropical mode waters suggest that dust deposition may have also increased in the western basin. Our observations are consistent with recent reports linking increasing sea surface temperatures in the tropical North Atlantic to increased removal of atmospheric dust via precipitation over the past several decades and highlight the importance of accurate representation of dust deposition processes for modelling Fe biogeochemistry.

## 1. Introduction

Constraining the supply of iron (Fe) to the ocean euphotic zone is of critical importance due to the role of Fe as an essential trace nutrient for ocean primary productivity. Changes in the supply of Fe to the surface ocean modify ocean uptake of $CO_2$, impacting global climate through modulation of atmospheric $CO_2$ levels. Inputs of new Fe can be supplied to the ocean by advection from continental margin sediments, riverine inputs, and hydrothermal fluxes (Boyd and Ellwood, 2010 and references therein), although in many remote ocean regions, the primary input of new Fe to the euphotic zone is deposition of atmospheric aerosols (Duce and Tindale, 1991; Jickells et al., 2005; Krishnamurthy et al., 2010). This exchange between the atmosphere and the ocean must be better constrained in order to accurately model the biogeochemical cycling of biologically-important trace metals in the ocean and its feedbacks on global climate.

Estimates of dust deposition and associated Fe flux to the open oceans made from measurements of dust flux at coastal and island-based sampling sites have greatly informed our knowledge of ocean dust deposition rates and have constrained atmospheric sources of trace metals to the upper ocean (Duce and Tindale, 1991; Duce et al., 1991). However, direct measurement of dust flux on spatial and temporal scales necessary to fully characterize aerosol dust inputs to the open ocean and their sensitivity to changing global climate is logistically infeasible. To address this challenge, upper-ocean distributions of various trace metal species have been employed as chemical tracers of integrated atmospheric dust deposition on the ocean over timescales of weeks to years, including dissolved Al (Measures and Brown 1996; Measures and Vink, 2000), dissolved Ti (Dammshäuser et al., 2011), and particulate Al, Fe, and Ti (Bory and Newton, 2000; Barrett et al., 2012; Dammshäuser et al., 2013).

In the North Atlantic, mineral dust aerosols are the dominant source of Fe to the euphotic zone in open-ocean regions, supplied by atmospheric deposition of dust from the Saharan and Sahel deserts transported across the Atlantic basin by prevailing easterly winds (Jickells et al., 2005; Ussher et al., 2013; Conway and John, 2014). In 2003, a coupled ocean-atmosphere trace-metal sampling program was carried out as part of the CLIVAR/$CO_2$ Repeat Hydrography Program occupation of section A16N in the eastern North Atlantic (Measures et al., 2008a; Buck et al., 2010a,b; Barrett et al., 2012, 2014). Sampling along A16N was repeated in 2013, which to our knowledge represents the completion of the first repeat high-resolution, basin-scale trace metal section, providing the opportunity to examine how ocean trace metal inventories have responded to both short-term variability and decadal-scale trends in dust deposition. Here, we compare the measured concentrations of dissolved Al and particulate Al and Fe along A16N in 2003 and 2013 to determine how features in oceanic trace-metal distributions have

changed between the two occupations of the section; because of the distinct biogeochemical cycling of dissolved Fe in the upper ocean, discussion of dissolved Fe concentrations are beyond the scope of this paper and will be the subject of a separate, future manuscript. We examine changes in aerosol dust loading over the North Atlantic reported from satellite observations and model output to determine how changes in ocean trace metal inventories are related to trends in the atmospheric dust cycle and to better understand the relative importance of dust generation, atmospheric transport patterns, and deposition processes in controlling the delivery of trace metals to the North Atlantic. Repeat observations of upper-ocean trace metal distributions have important implications for the use of dust transport models to predict future trends in Fe deposition on the oceans and for validation of model representations of dust transport and deposition processes under changing dust conditions.

## 2. Methods

### *2.1. Sample collection*

The trace metal data used in this analysis were collected during two sampling efforts along CLIVAR/$CO_2$ Repeat Hydrography section A16N from Reykjavik, Iceland to Natal, Brazil (**Fig. 1**) that took place from 20 June to August 7 2003 and from 3 August to 3 October 2013. Trace metal sampling was done at 60 and 63 stations in 2003 and 2013, respectively, with typical spacing of ~60 nm, or ~1 degree of latitude between stations (Fig. 2). Seawater was collected from the surface to depths of approximately 1000 m using 12 L GO-FLO bottles on a trace metal-clean rosette. GO-FLO bottles were sub-sampled in a clean laboratory van equipped with a HEPA filtered air system (see Measures et al. 2008b for details). Sub-sampling protocols and dissolved and particulate trace metal analyses have been described previously for the 2003 dataset (Measures et al., 2008a; Barrett et al., 2012) and were repeated in 2013. Briefly, subsamples for dissolved trace metal analysis were collected by pressure-filtering seawater (<55 kPa filtered, compressed air) through acid-washed, 0.4 µm polycarbonate track-etched filters in polypropylene filter holders. Suspended particulate-matter samples collected on the filters were rinsed with deionized water (adjusted to pH 8 with ammonium hydroxide) while on the filter holder with a low vacuum applied. Mixed cellulose ester backing filters were used to ensure even sample loading. Filtration was started ~30 to 60 minutes after sample collection and was generally completed within 1 hour. The average sample filtration volume was 8.0 $\pm$ 2.2 and 8.9 $\pm$ 2.1 L in 2003 and 2013, respectively. Although the sampling protocol should minimize any effects of particle settling by virtue of the shallow cast depths and short times between sample collection and filtration, losses from particle settling are not quantified and both the 2003 and 2013 datasets could underestimate actual

particulate trace metal concentrations. In 2003, sampling depths were limited to the upper 750 m between 62 and 27°N due to problems with the load-handling ability of the winch.

One change to sample collection in 2013 was the addition of a piece of acid-cleaned Teflon tubing to the interior of the GO-FLOs that attached to the stopcock and curved down to fit against the opposite side of the bottle with a beveled edge, as described by Cutter and Bruland (2012) and Planquette and Sherrell (2012). The modification was made to facilitate draining of the entire bottle during particle sampling, including the small volume below the level of the stopcock. However, we must consider potential sampling artifacts introduced by addition of the tubing. If particle settling in the bottle was significant, the Telfon tubing could have allowed collection of particles at the bottom of the GO-FLO that would not have been captured during sampling in 2003. However, previous studies have concluded that this GO-FLO modification does not significantly counteract effects of particle settling (Planquette and Sherrell, 2012). Additionally, we would expect particle settling effects to be greatest in mid- and high-latitude surface waters where high seasonal biological production would lead to large, rapidly-sinking aggregates. As will be discussed below, no significant increases in particulate trace metal concentrations were observed in these regions in 2013 compared to 2003. Instead, the largest changes were observed at low latitudes where particle disaggregation and degradation processes dominate and likely result in a pool of small suspended particles (Barrett et al., 2012; 2014). Thus, it is improbable that the differences in particulate trace metal distributions between 2003 and 2013 could be the result of a sampling artifact introduced by modification of the GO-FLO bottles.

*2.2. Analytical methods*

Subsamples of filtered seawater (<0.4 μm) were collected into acid-washed 100 mL LDPE bottles, acidified to 0.024M HCl, and analyzed for dissolved Al concentrations using the flow injection method of Resing and Measures (1994). The method had a detection limit of 0.5 nM with a precision of 3.0% in 2003 and a detection limit of 0.3 nM with a precision of 3.0% in 2013. Three SAFe and two GEOTRACES reference standards were run regularly and compared to consensus values for quality assurance and control in 2013 (**Table 1**).

The trace metal composition of suspended particulate matter samples was determined by energy-dispersive X-ray fluorescence (ED-XRF) at NOAA/PMEL on a Thermo Fisher Quant'X equipped with a Rhodium Target X-Ray tube and an electronically cooled, lithium-drifted solid state detector using thin-film principles under a vacuum atmosphere. The ED-XRF protocol follows the methods of Feely et al. (1991) and has been described previously by Barrett et al. (2012). Analytical accuracy of the ED-XRF

analysis is confirmed by analysis of certified reference material NIST SRM 2783, air particulate on filter media, which shows good agreement (+/- 8%) between certified and measured values for Al and Fe (Barrett et al., 2012). Minimum detection limits for *in situ* seawater concentrations of particulate Al and Fe are 0.54 nM and 0.03 nM, respectively, given an average sample filtration volume of 8 L. Minimum detection limits are determined from a standard of known concentration and are defined as:

$$MDL = (3 \cdot \sqrt{I_b}) / (I_p / c)$$

where $I_b$ is the background intensity, $I_p$ is the peak intensity, and $c$ is the concentration of the standard. Method-blank values of 11.0 and 2.1 ng/cm$^2$ for Al and Fe, respectively, were determined from analysis of acid-cleaned filter blanks and subtracted from measured sample values (Barrett et al., 2012). Precision of the XRF analyses was typically 3–11% for particulate Al and 4–8% for particulate Fe.

To account for differences in both station and depth spacing in the sampling plans for the two occupations of A16N, concentrations of particulate Fe, particulate Al and dissolved Al were subjected to a linear interpolation onto an evenly-spaced grid to compare the trace metal distributions between the 2003 and 2013. Difference plots were restricted to regions of sampling overlap between the two cruises at latitudes 2°S to 62°N. To determine average trace metal concentrations in features of interest along the transect, a Monte-Carlo type simulation (n=1000) was performed by randomly varying the sample data within the bounds of individual measurement uncertainties and calculating an average concentration for the region of interest in each interpolated concentration field. The non-parametric Kolmogorov-Smirov test (Massey, 1951) was applied to determine the significance of differences between the distribution of means calculated for each region by the Monte-Carlo approach for 2003 and 2013.

## 3. Results and discussion

### 3.1 Changes in particulate Al and Fe concentrations along A16N

#### *3.1.1 Distributions of particulate Al and Fe in 2003 and 2013*

The distributions of particulate Al (pAl) and particulate Fe (pFe) in the upper 1000 m along CLIVAR A16N in 2003 and 2013 are shown in **Fig. 2**. The major features of both the pAl and pFe distributions that were reported in 2003 (Barrett et al., 2012) were also observed along the section in 2013, and are briefly described below.

At high-latitude stations, high pAl concentrations in surface waters result from mixing with river outflow from southern Iceland that carry high sediment loads. Re-suspension of sediments from shallow bottom depths over the Icelandic shelf can be seen in the deep pAl maxima in vertical profiles at these stations. Surface pAl concentrations are also elevated by scavenging of dissolved Al onto biogenic particles in productive coastal waters and, in 2003, in mid-latitude surface waters (~40–55°N) following the spring bloom in the North Atlantic. Concentrations of pAl are relatively low throughout the subtropical gyre, reflecting low rates of dust deposition on surface waters. In the tropical North Atlantic between ~10 and 20°N, pAl concentrations in surface waters are high (6–11nM) due to intense seasonal aerosol dust deposition. Shipboard daily-integrated aerosol samples collected in 2003 (Buck et al., 2010a) and 2013 (Shelley, unpublished data) show peak concentrations of aerosol Al over a similar latitudinal range. Spatial patterns in the transport of aerosol dust across the tropical North Atlantic are largely controlled by the migration of the Intertropical Convergence Zone (ITCZ) and the distribution of peak surface-ocean pAl and aerosol Al flux observed in both A16N occupations is consistent with the northerly shift in aerosol transport expected in Northern hemisphere summer (Husar and Prospero, 1997). The most prominent feature in the pAl distribution is a large subsurface region of elevated pAl concentrations (up to 20 nM in 2003 and 31 nM in 2013) that extends from 200 m down to maximum sampling depths (1000 m) between the equator and 20°N. This subsurface pAl maximum develops as aerosol dust particles deposited on surface waters settle through the upper water column and lithogenic particulate Al is released at depth during disaggregation and degradation of large sinking particles and biological aggregates. The spatial extent of this feature spans the full annual latitudinal range of peak dust transport from the African continent to the North Atlantic (Husar and Prospero, 1997). There is no evidence of sedimentary influence on trace metal concentrations at this distance from the African continent. Tracers of sedimentary inputs such as dissolved Mn and 228Ra are confined to regions within ~500 km of the coast (Hatta et al., 2014) and mineralogical assessment of particles has demonstrated that dust is the principal source of lithogenic material to the upper water column at these latitudes (Ohnemus and Lam, 2014).

Generally, concentrations of pFe along A16N (**Fig. 2d,e**) have a distribution similar to pAl as both trace metal species are supplied largely from the same lithogenic sources (primarily aerosol dust) and are subject to similar removal processes (aggregation and sinking) in the upper water column of the North Atlantic. High concentrations of pFe introduced to surface waters from fluvial sources and at depth from shelf and bottom sediments can be seen in high-latitude pFe profiles. Maximum surface-

ocean pFe concentrations at low latitudes (~10–20°N) result from intense seasonal deposition of Saharan dust and are consistent with shipboard estimates of the location of maximum aerosol Fe concentrations during A16N in both 2003 and 2013 (Buck et al., 2010a; Shelley, unpublished data). The pFe distribution also indicates the presence of a large subsurface particulate plume at low latitudes that develops, in part, from export of dust deposited on overlying surface waters. However, unlike Al, Fe also undergoes strong biological cycling in the upper water column with uptake of dissolved Fe in the surface ocean and remineralization below the euphotic zone. At low latitudes (0–20°N) along A16N, dissolved Fe released by remineralization of sinking organic matter accumulates at depth in poorly-ventilated, low-oxygen waters below the euphotic zone. These waters are depleted in dissolved Fe relative to nitrate and remineralized carbon as inferred from AOU, suggesting relatively strong removal of dissolved Fe by scavenging onto particles (Measures et al., 2008a; Hatta et al., 2014). Hence, in addition to the vertical transport of dust particles, scavenging of the dissolved Fe pool likely also contributes to the high concentrations observed at depth in pFe profiles under the Saharan dust plume.

*3.1.2. Differences between 2003 and 2013 particulate Al distributions along A16N*

Differences in the distributions of pAl in the upper water column between 2003 and 2013 are primarily due to changing lithogenic inputs to the open ocean, largely aerosol dust fluxes, and variability in processes that control particle dynamics in the ocean interior. We focus on two regions where differences in measured pAl concentrations between the 2003 and 2013 occupation of A16N are greatest: surface waters in the productive mid-latitudes and in the equatorial region under the atmospheric outflow of Saharan dust.

First, as shown in **Fig. 2c,** pAl concentrations in mid-latitude surface waters (~40–50°N) were lower (typically by > 5nM) than measured in 2003. While most pronounced in the surface ocean, pAl concentrations were also lower throughout the upper 1000 m in this region. In 2003, sampling occurred shortly after the onset of the North Atlantic spring bloom at these latitudes (Henson et al., 2009), where high concentrations of biogenic particles, primarily diatoms, are known to scavenge the surface-ocean dissolved Al pool accumulated from dust deposition over winter months (Kremling and Hydes, 1988; Moran and Moore, 1988). This seasonal scavenging of dissolved Al is the probable source of the high pAl concentrations (up to 12.2 nmol $L^{-1}$) observed in surface waters in 2003 (Barrett et al., 2012), as well as elevated pAl at depth as biogenic particles are exported out of the surface ocean (**Fig. 2a**). The absence of this pAl feature in 2013 (**Fig. 2b**) is most likely due to the difference in the timing of sampling (~6 weeks later in the year) compared to the 2003 occupation of A16N. Rapid sinking rates for POC (100–

160 m $d^{-1}$; Lochte et al., 1993) and diatom aggregates (~75 m $d^{-1}$; Briggs et al., 2011) have been observed following the spring bloom in the subpolar North Atlantic during the 1989 JGOFS North Atlantic Bloom Experiment (NABE) and North Atlantic Bloom 2008 experiment (NAB08), respectively. By the time sampling commenced along A16N in 2013 (early August), high seasonal, bloom-induced pAl concentrations had likely already dissipated due to bloom decay and particle export. As shown in Fig. 3 for a repeat station at 45°N, an intense surface-ocean particulate Si maximum (>350 nM) in 2003 coincides with elevated pAl concentrations in the surface ocean (up to 8 nM) and at depth (>4 nM). Differences in the behavior of particulate Si and Al with depth reflects their differential remineralization (e.g., Measures et al., 2014). In contrast, low surface ocean particulate Si concentrations (<50 nM) in 2013 suggests absence of bloom activity and low pAl concentrations are observed throughout the water column (<2 nM).

The largest differences in pAl between 2003 and 2013 were observed in the subtropical and equatorial North Atlantic (**Fig. 2c)**. Here, upper water column pAl distributions primarily reflect deposition of aerosol dust from the deserts of northern Africa (Buck et al., 2010a). In 2013, increased pAl concentrations were observed within the broad subsurface (>200 m) particulate plume at low latitudes that results from vertical transport of aerosol dust particles through the upper water column. At depths >200 m between 0 and 20°N, the average pAl concentration increased by 1.6 nM (14%) from a calculated mean of 11.5 $\pm$ 0.2 nM in 2003 to 13.1 $\pm$ 0.6 nM in 2013 (two-sample Kolmogorov-Smirov test, $\alpha$<0.01).

A residence time of 1–4 years for this subsurface particulate feature can be calculated using average ocean pAl concentrations (Barrett et al., 2012 and this work), concentrations of total aerosol Al measured along A16N (Buck et al. 2010a; Shelley, unpublished data), an aerosol Al solubility of 10% for Saharan aerosols (Buck et al., 2010a), and an average aerosol deposition velocity of 1.2 cm $s^{-1}$, which is close to the estimate of Duce et al. (1991). Estimates for aerosol deposition velocities are not well constrained and this value adds uncertainty to our estimate of pAl residence time. For example, a recent study by Niedermeier et al. (2014) measured mean aerosol deposition velocities of 0.2 cm $s^{-1}$ for 1–10 µm mineral dust particles in the tropical northeast Atlantic, similar to the distribution of particle size in the A16N Saharan aerosol samples (Buck et al., 2010b). Using the aerosol deposition velocity measured by Niedermeier et al. would increase residence times by up to a factor of 6 and thus our calculations are likely a conservative estimate.

Climatological estimates of dust flux to the surface ocean at these latitudes (2–20 g dust $m^{-2}$ $yr^{-1}$) (Zender et al., 2003; Jickells et al., 2005; Mahowald et al., 2005) combined with an aerosol Al content of

8.0% (Wedepohl, 2005) generate similar estimates of residence time (<1 to 3 years). Multi-year residence times for pAl in the upper 1000 m is likely an effect of small particle size. This region is a zone of intense remineralization as evidenced by a high AOU, nitrate, and dissolved Fe (Measures et al., 2008; Hatta et al. 2014). Small lithogenic particles delivered by aerosol deposition, typically are likely released at depth to the suspended matter pool as aggregates are subjected to remineralization and degradation processes. A decrease in the mean lithogenic particle size over the decade interval could increase the residence time of suspended particulate matter and result in the observed increase in ocean pAl concentrations. However, studies of the properties of Saharan aerosols over our study period show no indication that the mean particle size of lithogenic inputs to this region has decreased (Ryder et al., 2013). Thus, observed pAl concentrations in the subsurface maximum at low latitudes represent a multi-year average signal of annual dust deposition and the increase in average pAl concentrations in this large-scale feature suggests an increase in dust deposition to surface waters in this region between 2003 and 2013.

Concentrations of pAl reach maximum concentrations in equatorial surface waters (10.9 nM in 2003 and 11.2 nM in 2013) at latitudes under the Saharan dust outflow (~0–20°N). If aerosol deposition to surface waters in this region increased between the two occupations of A16N as suggested from changes observed in the large particulate plume deeper in the water column, it may be expected that surface-ocean pAl concentrations would also be higher in 2013. However, the differences in average pAl concentrations between 2003 and 2013 in the mixed layer are less robust (typically <0.5nM), which is likely a result of the variability in dust deposition and the very short residence times expected for particles in the surface layer. A residence time for surface-ocean particulates in the equatorial North Atlantic can be calculated from surface inventories (<50 m) of pAl in both 2003 and 2013 and the measured and climatological aerosol input parameters described above. Resulting residence times are generally 1–5 weeks, although estimates range up to a maximum of 43 weeks due to the high degree of variability in aerosol deposition events. At the lower end, our estimate is comparable to previous work reporting residence times of 3–22 days for pAl in the equatorial North Atlantic from upper water column pAl concentrations and climatological dust fluxes (Dammshäuser et al., 2013) and a lithogenic particle residence time of 10–40 days in the subtropical North Atlantic using sediment trap data (Bory and Newton, 2000). This short residence time implies that surface-ocean particulate trace metal concentrations will be strongly influenced by the highly episodic nature of dust transport over the North Atlantic.

*3.1.3. Differences between 2003 and 2013 particulate Fe distributions along A16N*

Similar to the changes in pAl distributions along A16N between the two occupations, the largest differences in the pFe distribution between 2003 and 2013 were also observed in the subsurface particulate maximum in the equatorial North Atlantic (**Fig. 2f)**. Between the equator and 20$^{o}$N at depths below 200 m, average pFe concentrations increased by 0.9 nM (27%) from a calculated mean of 3.4 $\pm$ 0.02 nM in 2003 to 4.3 $\pm$ 0.02 nM in 2013 (two-sample Kolmogorov-Smirov test, $\alpha$ <0.01).

Inputs of pFe and pAl are expected to be closely coupled in this region given the strong atmospheric source common to both metals. Considering pAl as a proxy for lithogenic dust inputs, the increase in pFe (+27%) relative to pAl (+14%) between 2003 and 2013 suggests that vertical transport of dust particles would account for approximately half of the observed increase in pFe concentrations. The excess pFe at depth observed in 2013 could be due to increased scavenging of the high concentrations of subsurface dissolved Fe in this region (up to 2 nM in 2003; Measures et al., 2008a). We observe a significant increase in Fe:Al molar ratio of particles in the subsurface plume (0.29 $\pm$ 0.01 in 2003 and 0.32 $\pm$ 0.3 in 2013; p<0.01), implying changes in the internal cycling of Fe in the equatorial North Atlantic. For example, scavenging is known to be important in controlling the partitioning of remineralized Fe between dissolved and particulate phases in subsurface waters this region (Measures et al., 2008; Hatta et al., 2014) and could contribute to the changes in pFe observed been 2003 and 2013. Increased scavenging pressures could result from higher lithogenic particle loads in 2013. Likewise, average particulate P concentrations in this region more than doubled in 2013 compared to 2003 (supplementary data Fig. S1), indicating a higher concentration of biogenic particles, which are also efficient at scavenging dissolved Fe (Balistrieri et al., 1981). While we cannot yet compare dFe distributions along A16N between 2003 and 2013, maximum dFe concentrations observed in the top 1000 m in 2003 (Measures et al., 2008) are typically higher (1.26–2.02 nM, 13 stations) than those observed in 2008 (0.98–1.47 nM, 6 stations; *R/V Oceanus* OC 449-2) by Fitzsimmons et al. (2013) in regions of sampling overlap, (6–18°N, 25–31°W), which would be consistent with an increase in scavenging rates.

It is unlikely that a change in the composition of aerosol sources between 2003 and 2013 could explain the increase in the Fe:Al ratios of ocean particulate matter. Analysis of aerosol samples collected daily along A16N suggests that the Fe:Al ratio of aerosol dust inputs to this region may have declined between the two occupations (0.32 $\pm$ 0.05 in 2003 and 0.27 $\pm$ 0.2 in 2013, p<0.01; Buck et al., 2010; Shelley, unpublished data). Given the highly episodic nature of aerosol transport and the short collection time for these samples, this difference may or may not accurately reflect long-term trends in aerosol

composition, but these samples provide no evidence for an increase in the Fe:Al ratio of source aerosols that would explain the changes observed in the chemistry of ocean particulate samples.

In efforts to compare our A16N timepoints to other datasets , we also consider particulate Al and Fe data collected during the 2010/2011 GEOTRACES North Atlantic Zonal Transect, between our two occupations of A16N (Ohnemus and Lam, 2014; Twining et al., 2014). The intersection between these two transects in the region of interest in the equatorial North Atlantic occurs at approximately 19°N and 29°W, a location with high spatial gradients in dust transport and deposition, and at the interface between two distinct water masses at intermediate depths (supplementary data Fig. S5); these factors may introduce additional variability to particulate trace metal measurements (supplementary data Fig. S2). Additionally, methodological differences in sample collection further complicate data comparison. Particulate sampling by Ohnemus and Lam (2014) employed a 0.8 µm minimum filter size as compared to the 0.4 µm filter used during both A16N occupations. We note the significant differences between particulate Al concentrations at depth (>200 m) at open-ocean stations in the eastern North Atlantic from 0.8 µm filter samples and 0.45 µm filter samples collected during the GEOTRACES section (Twining et al., 2014; supplementary data Fig. S3). Hence, we conclude that methodological differences preclude meaningful comparison of these two datasets.

### 3.2 Changes in dissolved Al concentrations along A16N

#### *3.2.1. Distribution of dissolved Al*

The distribution of dissolved Al (dAl) in the upper 1000 m of the water column along A16N in 2013 is broadly similar to that observed a decade earlier (**Fig. 4;** Measures et al., 2008; Barrett et al., 2012); these general features are briefly described below.

Surface-ocean dAl concentrations reflect input of Al from the deposition and partial dissolution of atmospheric aerosols and removal by particle scavenging processes. The dAl surface maxima observed at low latitudes (~0–10°N) result from intense seasonal deposition of aerosol dust on the surface ocean in the equatorial North Atlantic. Outside of the equatorial region, surface concentrations of dAl are much lower, reflecting reduced dust inputs. At mid-latitude stations, scavenging of dAl onto biogenic particles following the spring bloom in the North Atlantic (see discussion in section 3.1.2) leads to strong removal of dAl from surface waters as Al is transferred to the particulate phase; thus dAl profiles exhibit minimum values at the surface. There are two subsurface features in the dAl distribution that result from subduction of Al-rich surface waters. The first is the local maximum in dAl concentrations (>23 nM in 2003 and >25 in 2013) centered at depths of ~300 m in subtropical waters

(20–35°N). This signal originates from the subduction of dust-imprinted waters in the western basin that form the Atlantic subtropical mode waters. Similarly, deposition of Saharan dust on the Mediterranean basin leads to Al-rich surface waters that are subducted and transported through the Strait of Gibraltar as Mediterranean outflow water (MOW). The CLIVAR A16N section transects the MOW at 35–41°N where elevated dAl concentrations were observed at depths below ~700 m during both occupations, as indicated by the local salinity maximum (Measures et al., 2008a). At more northerly stations along A16N (>40°N), minimum dAl values at the surface and increasing dAl with depth reflect the strong removal of dAl from the surface mixed layer by seasonal scavenging pressures from high concentrations of biogenic particles as described in section 3.1.2.

*3.2.2. Differences between 2003 and 2013 dissolved Al distributions*

Similar to the changes observed in pAl and pFe, increased concentrations of dAl were observed in 2013 in regions heavily impacted by delivery of aerosol dust from low-latitude continental sources in surface waters in the tropical North Atlantic (0–20°N) and where A16N intersects subtropical mode waters (**Fig. 4c**).

The largest differences in the dAl distribution between the two occupations of A16N are found in North Atlantic equatorial surface waters (0–20°N) where high rates of dust deposition and the partial dissolution of aerosol Al lead to local maxima in surface-ocean dAl concentrations (Measures et al., 2008a). Maximum dAl concentrations observed in this region increased from 36 $\pm$ 1.1 nM in 2003 to 42 $\pm$ 1.3 nM in 2013 and average dAl concentrations in the upper 50 m increased by 3.1 nM (16%) from 19.5 $\pm$ 0.02 nM in 2003 to 22.6 $\pm$ 0.2 nM in 2013. Atmospheric dust transport across the equatorial North Atlantic is controlled spatially by the seasonal shift in the ITCZ, which is centered approximately between the equator and 10°N during boreal winter and farther north between 10 and 20°N during summer (Husar and Prospero 1997). The residence time of surface-ocean dAl in the eastern tropical North Atlantic has been estimated to be on the order of several months from both seasonal observations and modeling work (Helmers and van der Loeff, 1993; Dammshäuser et al., 2011; van Hulten et al., 2013). Due to its relatively short residence time, dAl accumulates in surface waters from 0 to 10°N in the winter then slowly decays in this region over the summer as the location of maximum dust deposition shifts north, as can be seen in the seasonal observations of Helmers and van der Loeff (1993). Comparison of dAl profiles at 19°–21°N with dAl data of Measures et al. (2014) collected at similar latitudes during winter months on the 2011 GEOTRACES NAZT also illustrates the response of surface-ocean dAl concentrations to the seasonality of dust inputs to this region (supplementary data

Fig. S4); subsurface features in these dAl profiles reflect local boundaries between intermediate-depth water masses (supplementary data Fig. S5).

Because of the lag of ~6 weeks between the timing of sampling in 2003 and 2013, dAl surface concentrations between 10–20°N in 2013 could be higher due to extended exposure to summertime aerosol deposition. However, if aerosol inputs were constant between 2003 and 2013, dAl concentrations over 0–10°N would be expected to be lower in 2013 due to a longer time for particle scavenging to remove dAl from surface waters after local inputs ceased. Instead, comparison of the 2003 and 2013 dAl distributions shows an increase in average surface concentrations over 0–10°N as well (3 nM). It is unlikely that reduced scavenging pressures could explain the persistence of the dAl signal given the increased particulate trace metal loading discussed above. Hence, the increase in average dAl concentrations observed in 2013 compared to 2003 in surface waters (>50 m) between the equator and 20°N is most likely the result of increased atmospheric dust deposition in 2013 compared to 2003. Due to the relatively short residence time of surface-ocean dAl in this region, concentration differences can be attributed solely to inter-annual variability in dust deposition (Prospero and Lamb, 2003). However, the sign and magnitude of the observed change is consistent with the long-term trend of increasing dust deposition across the equatorial North Atlantic suggested by the particulate Al and Fe.

Increased dAl concentrations between 2003 and 2013 are also observed along potential density surfaces $\sigma_\theta$ = 26.5 to 26.9 (approximately 200–400 m) in the core of the subtropical mode water along A16N between 25 and 35$^o$N (**Fig. 5**). Increased dAl concentrations in these mode waters suggest that dust deposition to surface waters may have been higher in the western North Atlantic during mode water formation. Long-range transport of Saharan dust across the North Atlantic is a major contributor to atmospheric aerosol loading over the western North Atlantic (Li et al., 1996; Prospero and Lamb, 2003; Prospero and Mayol-Bracero, 2013) and Saharan dust deposition is a major source of trace metals, notably Al, to subtropical surface waters in the western Atlantic basin (Jickells 1999). The average increase in dAl in the subtropical mode water signal (1.0 nM, 5%) is smaller than the relative increases in particulate (+14%) and dissolved (+16%) Al observed in the equatorial region along the A16N transect, which result from local dust deposition in the eastern basin rather than transit of dAl-imprinted water masses. This variation could be due to real differences between the dust transport pathways or deposition processes in the eastern and western Atlantic. Although the residence time of subtropical mode waters in the North Atlantic is relatively short (~4 years; Trossman et al., 2012), the transit time of subducted mode waters from their origin in the western basin could contribute to differences between dAl inventories of local and advected water masses. Additionally, the residence time of surface-ocean

dAl in the region of mode water formation in the western basin is likely at least twice as long as the residence time of either the dAl or pAl signal in the eastern basin; thus subtropical mode water dAl may also reflect changes in dust deposition over the longer integration period in mode water source regions. In regions of the western Atlantic where formation of North Atlantic subtropical mode water occurs (Hanawa and Talley, 2001; Kelly and Dong, 2013), model output estimates the residence time of surface-ocean dAl to be 4–20 years (Gehlen et al., 2003; Han et al., 2008). After subduction in the western basin, dAl in this water mass is subject to greatly reduced particle scavenging pressures, leading to semi-conservative behavior of dAl in subsurface waters (Orians and Bruland, 1986; Measures and Edmond, 1990).

Elevated dAl concentrations are also observed in the high-salinity Mediterranean outflow water (MOW) at ~700–1100 m between 35 and 41°N along A16N during both occupations. Due to restrictions on sampling depth at these stations, the 2003 occupation sampled the upper portion of this water mass but missed the core of the signal, making potential changes in the dAl concentrations in this water mass difficult to discern. In 2013, dAl concentrations in the core of the MOW (800–1000 m) reached a maximum of 29.5 nM. Concentrations of dAl in the MOW during the 2013 occupation of A16N are comparable to previous observations of dAl maxima in the MOW in the eastern subtropical North Atlantic (**Fig. 6**). The variability in dAl concentrations between the A16N data and previous studies likely primarily reflects spatial differences in sampling sites and the dilution of MOW with low-Al North Atlantic Central Water as it moves along northern and westward flow branches through the eastern North Atlantic (Lozier et al., 1995). Satellite observations of aerosol distributions and aerosol sampling at ground-based sites throughout the Mediterranean basin indicate that Saharan dust inputs vary temporally and spatially on relatively short timescales, largely controlled by changes in atmospheric circulation patterns with robust correlation with the summer North Atlantic Oscillation index (Moulin et al., 1998; Dayan et al., 2008). Previous studies have reported that dust transport to the Mediterranean decreased between the mid-1980s to the late 1990s, increased from the late 1990s to the mid-2000s, and shows a negative trend from the mid-2000s to 2011 (Ridame et al., 1999; Antoine and Nobileau, 2006; Pey et al., 2013). However, these trend reversals in dust deposition to the Mediterranean have occurred on much shorter periods than the timescale of deep water circulation in the Mediterranean basin, which is on the order of several decades (Chou and Wollast, 1997) and controls dAl concentrations in the MOW. Hence, the long residence time of Al-enriched water in the Mediterranean basin would, to a large extent, likely integrate any variability in aerosol Al input to Mediterranean surface waters.

### 3.3. Trends in atmospheric dust transport over the equatorial North Atlantic Ocean

In **Fig. 7**, the trace metal data from the subsurface particulate plume at low latitudes (pAl and pFe), surface waters in the tropical North Atlantic (dAl), and North Atlantic subtropical mode waters (dAl) are plotted for both 2003 and 2013, showing the increase in both mean and maximum trace metal concentrations observed for each region. **Table 2** summarizes estimated residence times for pAl, pFe, and dAl features in equatorial and subtropical North Atlantic heavily impacted by the deposition of atmospheric dust from the deserts of northern Africa and the average change in trace metal concentrations observed for each feature between 2003 and 2013. Increased inventories of these trace metal species suggest that dust deposition to the eastern tropical North Atlantic increased between 2003 and 2013. These differences reflect a combination of inter-annual variability and the decadal trend in dust deposition that will vary with the residence time of the trace metal signal considered.

Because of the importance of atmospheric aerosols and their feedbacks in the climate system, observational efforts have greatly expanded over the last several decades and have resulted in availability of records of global aerosol distributions from various satellite products (e.g., MODIS, AVHRR, SeaWiFS, EOS, TOMS, MISR) and ground-based aerosol sampling networks (e.g., AERONET, IMPROVE) (Chin et al., 2013). The changes in the average global aerosol loading over the last several decades detected from satellite products are small relative to the total aerosol loading and recent analyses have disagreed on the size and direction of change in average global aerosol transport (Mishchenko et al., 2007; Zhang and Reid, 2010; Hsu et al., 2012). However, many analyses have found robust regional trends in aerosol optical depth (AOD) due to changing local natural and anthropogenic sources. There is significant agreement among studies employing various satellite, ground-based sampling, and modelling products that dust transport across the tropical North Atlantic Ocean has decreased between the 1980s and late 2000s (Mishchenko and Geogdzhayev, 2007; Foltz and McPhaden, 2008; Wong et al., 2008; Zhao et al., 2008; Evan and Mukhopadhyay, 2010; Zhang and Reid, 2010; Hsu et al., 2012; Chin et al., 2013). These studies report negative AOD trends in regions over the tropical North Atlantic affected by African dust transport of -0.01 to -0.1/decade for the last 2 decades, although most estimates fall within -0.03 to -0.05/decade (Foltz and McPhaden, 2008; Zhao et al., 2008; Zhang and Reid, 2010; Hsu et al., 2012). Average annual AOD in our study region is estimated to be 0.3–0.5 (Foltz and McPhaden, 2008; Zhang and Reid, 2010; Chin et al., 2013), making the estimated decadal rate of AOD decline between 2 and 30%.

MODIS satellite images showing AOD over the North Atlantic integrated over the 2003 and 2013 cruise dates as well as for the preceding 12 months are shown in **Fig. 8**. Although aerosol transport is expected to be highly variable both seasonally and interannually, the decline in AOD over the tropical North Atlantic during the 2013 occupation of A16N compared to a decade earlier is consistent with the general trend of decreasing regional aerosol loads over the last several decades reported by the above studies. The trend of decreasing AOD over the tropical North Atlantic has been linked to reduced dust production, perhaps due to increased precipitation over regions of dust generation (Prospero and Lam, 2003; Foltz and McPhaden, 2008), greening of African deserts (Cowie et al., 2013), or changes in atmospheric circulation patterns (Wong et al., 2008; Hsu et al., 2012). Recent work has also found that decreased AOD over the tropical North Atlantic is closely associated with increased precipitation over the tropical North Atlantic Ocean (Chin et al., 2013). Hence, both dust generation in continental source regions and removal efficiency (precipitation) over the ocean are important controls on trends in dust AOD over the tropical North Atlantic.

The increased inventories of pAl, pFe, and dAl in the upper 1000 m along A16N between 2003 and 2013 we observe in this study suggests that aerosol dust deposition on surface waters increased over this timeframe as average AOD over the tropical North Atlantic has declined. Wet deposition of atmospheric aerosols is the primary mechanism for the delivery of trace metals to the open ocean in the tropical North Atlantic (Hand et al., 2004). Our repeat observations of trace metal distributions along A16N are consistent with the findings of Chin et al. (2013) that removal of aerosol dust by precipitation over the open ocean is contributing to declining AOD trends over the tropical North Atlantic Ocean over the last several decades. Indeed, despite evidence that dust generation in desert source regions may be declining, our repeat of the A16N line indicates that ocean trace metal inventories in the eastern North Atlantic have not declined as a result, but rather have increased by 5–15%. This is consistent with observations that aerosol deposition processes have intensified as the magnitude or spatial patterns of precipitation shift, likely driven by increasing sea-surface temperatures as suggested by a number of previous studies (Wong et al. 2008; Foltz and McPhaden, 2008; Wang et al., 2012; Chin et al., 2013).

## 4. Conclusions

Repeat trace metal observations along CLIVAR A16N have allowed us to examine changes in large-scale trace metal features in the equatorial and sub-tropical North Atlantic impacted by dust deposition on timescales of weeks to months (surface dAl) and over multiple years (subtropical mode water dAl and subsurface pAl and pFe), which suggest that dust deposition on surface waters likely

increased by up to 15% between 2003 and 2013. This increase in trace metal concentrations in the upper water column support recent observational work linking declining aerosol optical depth over the North Atlantic to increased removal via precipitation over the ocean, especially in the eastern North Atlantic. Discussion of future changes in the atmospheric delivery of biologically-important trace metals to the oceans, most notably Fe (e.g., Mahowald et al., 2009), have primarily made use of modeling studies examining predicted changes in the global dust transport stemming from changes in the spatial extent and emission strength of desert source areas (Mahowald and Luo, 2003; Tegen et al., 2004; Woodward et al., 2005; Mahowald, 2007). This work emphasizes the need to robustly link trends in atmospheric dust loading to deposition rates over the ocean by more accurately representing deposition mechanisms such as wet deposition in models, a need that has been previously highlighted by other researchers (e.g., Prospero et al., 2010; Schultz et al., 2012).

**Acknowledgements**

The authors gratefully acknowledge Randy Morton for assistance with trace metal sample collection during the 2013 A16N cruise along with the Captain and crew of the RV *Ronald H. Brown* and the NSF/NOAA-funded U.S. Repeat Hydrography Program, including Richard Feely, Molly Barringer, and John Bullister. We also thank Eric Ward for helpful discussions and two anonymous reviewers whose comments greatly improved this manuscript. This work was funded by NSF grants OCE-1260376 to JAR and OCE-1260287 to WML. This is JISAO publication #2371 and PMEL publication #4237.

## References


Antoine, D., Nobileau, D., 2006. Recent increase of Saharan dust transport over the Mediterranean Sea, as revealed from ocean color satellite (SeaWiFS) observations. J. Geophys. Res. 111, D12214.

Balistrieri, L., Brewer, P.G., Murray, J.W., 1981. Scavenging residence times of trace metals and surface chemistry of sinking particles in the deep ocean. Deep Sea Res. 28, 101–121.

Barrett, P.M., Resing, J.A., Buck, N.J., Buck, C.,S, Landing, W.M., Measures, C.I., 2012. The trace element composition of suspended particulate matter in the upper 1000 m of the eastern North Atlantic Ocean: A16N. Mar. Chem. 142–144, 41–53.

Barrett, P.M., Resing, J.A., Buck, N.J., Feely, R.A., Bullister, J.L., Buck, C.S., Landing, W.M., 2014. Calcium carbonate dissolution in the upper 1000 m of the eastern North Atlantic. Global Biogeochem. Cycles 28, 386–397.

Bory, A.J.-M., Newton, P.P., 2000. Transport of airborne lithogenic material down through the water column in two contrasting regions of the eastern subtropical North Atlantic. Global Biogeochem. Cycles 14, 297–315.

Boyd, P.W., Ellwood, M.J., 2010. The biogeochemical cycle of iron in the ocean. Nature Geosci. 3, 675–682.

Briggs, M., Perry, M.J., Ivona Cetinić, I., Lee, C., D'Asaro, E., Gray, A.M., Rehm, E., 2011. High-resolution observations of aggregate flux during a sub-polar North Atlantic spring bloom. Deep-Sea Res. I 58, 1031–1039.

Buck, C.S., Landing, W.M., Resing, J.A., Measures, C.I., 2010a. The solubility and deposition of aerosol Fe and other trace elements in the North Atlantic Ocean: observations from the A16N CLIVAR/CO2 repeat hydrography section. Mar Chem. 120, 57–70.

Buck, C.S., Landing, W.M., Resing, J.A., 2010b. Particle size and aerosol iron solubility: A high-resolution analysis of Atlantic aerosols. Mar. Chem. 120, 14–24.

Chin, M., T. Diehl, Q. Tan, J.M. Prospero, R.A. Kahn, L.A. Remer, H. Yu, A.M. Sayer, H. Bian, I.V. Geogdzhayev, B.N. Holben, S.G. Howell, B.J. Huebert, N.C. Hsu, D. Kim, D.L. Kucsera, R.C. Levy, M.I. Mishchenko, X. Pan, P.K. Quinn, G.L. Schuster, D.G. Streets, S.A. Strode, O. Torres, and X.-P. Zhao, 2013: Multi-decadal variations of atmospheric aerosols from 1980 to 2009: sources and regional trends. Atmos. Chem. Phys. Discuss. 13, 19751–19835.

Chou, L., Wollast, R., 1997. Biogeochemical behavior and mass balance of dissolved aluminum in the western Mediterranean Sea. Deep-Sea Res. II 44, 741–768.

Conway, T.M., John, S.G., 2014. Quantification of sources of dissolved iron to the North Atlantic Ocean using iron isotopes. Nature, 511, 212–215.

Cowie, S.M., Knippertz, P., Marsham, J.H., 2013. Are vegetation-related roughness changes the cause of the recent decrease in dust emission from the Sahel? Geophys. Res. Lett. 40, 1868–1872.

Cutter, G.A., Bruland, K.W., 2012. Rapid and noncontaminating sampling system for trace elements in global ocean surveys. Limnol. Oceanogr. Methods 1, 425–436.

Dammshäuser, A., Wagener, T., Croot, P.L., 2011. Surface water dissolved aluminum and titanium: tracers for specific timescales of dust deposition to the Atlantic? Geophys. Res. Lett, 38, 6–11.

Dammshäuser, A., Wagener, T., Garbe-Schönberg, D., Croot, P.L., 2013. Particulate and dissolved aluminum and titanium in the upper water column of the Atlantic Ocean. Deep-Sea Res. I 73, 127–139.

Dayan, U., Ziv, B., Shoob, T., Enzel, Y., 2008. Suspended dust over southeastern Mediterranean and its relation to atmospheric deposition. Int. J. Climatol. 28, 915–924.

de Jong, J.T.M., Boye, M., Gelado-Caballero, M.D., Timmermans, K.R., Veldhuis, M.J.W., Nolting, R.F., van den Berg, C.M.G., de Baar, H.J.W., 2007. Inputs of iron, manganese and aluminium to surface waters of the Northeast Atlantic Ocean and the European continental shelf. Mar. Chem. 107, 120–142.

Duce, R.A., Tindale, N.W., 1991. Atmospheric transport of iron and its deposition in the ocean. Limnol. Oceanogr. 36, 1715–1726.

Duce, R.A., et al., 1991. The atmospheric input of trace species to the world ocean. Global Biogeochem. Cycles 5, 193–259.

Evan, A.T., Mukhopadhyay, S., 2010. African Dust over the Northern Tropical Atlantic: 1955–2008. J. Appl. Meterorol. Climatol. 49, 2213–2229.

Feely, R.A., Massoth, G. J., Lebon, G.T., 1991. Sampling of marine particulate matter and analysis by X-ray fluorescence spectrometry. *Marine Particles: Analysis and Characterization, Geophys. Monogr.*, No. 63, Amer. Geophys. Union, 251–257.

Fitzsimmons, J.N., Zhang, R., Boyle, E.A., 2013. Dissolved iron in the tropical North Atlantic Ocean. Mar. Chem. 154, 87–99.

Foltz, G.R., McPhaden, M.J., 2008. Trends in Saharan dust and tropical Atlantic climate during 1980–2006. Geophys. Res. Lett. 35, L20706.

Gehlen, M., Heinze, C., Maier-Reimer, E., Measures, C.I., 2003. Coupled Al-Si geochemistry in an ocean general circulation model: a tool for the validation of oceanic dust-deposition fields? Global Biogeochem. Cycles 17, 1028.

Han, Q., Moore, J.K., Zender, C., Measures, C., Hydes, D., 2008. Constraining oceanic dist deposition using surface ocean dissolved Al. Global Biogeochem. Cycles 22, GB2003, doi: 10.1029/2007GB002975.

Hanawa, K., Talley, L.D., 2001. Mode waters. *Ocean Circulation and Climate: Observing and Modelling the Global Ocean*, G. Sielder, J. Church, and J. Gould, Eds., Elsevier, 373–386.

Hand, J.L., Mahowald, N.M., Chen, Y., Siefert, R.L., Luo, C., Subramaniam, A., Fung, I. 2004. Estimates of atmospheric-processed soluble iron from observations and a global mineral aerosol model: Biogeochemical implications. J. Geophys. Res. 109, D17205.

Hatta, M., Measures, C.I., Wu, J., Roshan, S., Fitzsimmons, J.N., Sedwick, P., Morton, P., 2014. An overview of dissolved Fe and Mn Distributions during the 2010–2011 U.S. GEOTRACES north Atlantic Cruises: GEOTRACES GA03. Deep-Sea Res. II doi: 10.1016/j.dsr2.2014.07.005.

Helmers, E., van der Loeff, M.M.R., 1993. Lead and aluminum in Atlantic surface waters (50°N to 50°S) reflecting anthropogenic and natural sources in the eolian transport. J. Geophys. Res. 98, 20261–20273.

Henson, S.A., Dunne, J.P., Sarmiento, J.L., 2009. Decadal variability in North Atlantic phytoplankton blooms. J. Geophys. Res. 114, C04013.

Hsu, N.C., Gautam, R., Sayer, A.M., Bettenhausen, C., Li, C., Jeong, M.J., Tsay, S.-C., Holben, B.N., 2012. Global and regional trends of aerosol optical depth over land and ocean using SeaWiFS measurements from 1997 to 2010. Atmos. Chem. Phys. 12, 8037–8053.

Husar, R., Prospero, J., 1997. Characterization of tropospheric aerosols over the oceans with the NOAA advanced very high resolution radiometer optical thickness operational product. J. Geophys. Res. 102, 16899–16909.

Hydes, D.J., 1983. Distribution of aluminium in waters of the North East Atlantic 25°N to 35°N. Geochim. Cosmochim. Acta 47, 967–973.

Jenkins, W.J., Smethie, W.M., Boyle, E.A., Cutter, G.A., 2014. Water mass analysis for the U.S. GEOTRACES (GA03) North Atlantic sections. Deep-Sea Res. II doi:10.1016/j.dsr2.2014.11.018.

Jickells, T., 1999. Inputs of dust derived elements to the Sargasso Sea; a synthesis. *Mar. Chem.*, **68**, 5–14.

Jickells, T.D., An, Z.S., Andersen, K.K., Baker, A.R., Bergametti, G., Brooks, N., Cao, J.J., Boyd, P.W., Duce, R.A., Hunter, K.A., Kawahata, H., Kubilay, N., laRoche, J., Liss, P.S., Mahowald, N., Prospero, J.M., Ridgwell, A.J., Tegen, I., Torres, R., 2005. Global iron connections between desert dust, ocean biogeochemistry, and climate. Science 308, 67–71.

Kelly, K.A., Dong, S., 2013. The contributions of atmosphere and ocean to North Atlantic Subtropical Mode Water volume anomalies. Deep-Sea Res. II 91, 111–127.

Kramer, J., Laan, P., Sarthou, G., Timmermans, K.R., de Baar, H.J.W., 2004. Distribution of dissolved aluminium in the high atmospheric input region of the subtropical waters of the North Atlantic Ocean. Mar. Chem. 88, 85–101.

Kremling, K., Hydes, D., 1988. Summer distribution of dissolved Al, Cd, Co, Cu, Mn and Ni in surface waters around the British Isles. Cont. Shelf Res. 8, 89–105.

Krishnamurthy, A., Moore, J.K., Mahowald, N., Luo, C., Zender, C.S., 2010. Impacts of atmospheric nutrient deposition on marine biogeochemistry. J. Geophys. Res. 115, G01006.

673 Li, X., Marin, H., Savoie, D., Voss, K., Prospero, J.M., 1996. Dominance of mineral dust in aerosol light-
674 scattering in the North Atlantic trade winds. Nature 380, 416–419.
675
676 Lochte, K., Ducklow, H.W., Fasham, M.J.R., Stienen, C., 1993. Plankton succession and carbon cycling
677 47°N 20°W during the JGOFS North Atlantic Bloom Experiment. Deep-Sea Res. II 40, 91–114.
678
679 Lozier, M.S., Brechner Owens, W., Curry, R.G., 1995. The climatology of the North Atlantic. Prog.
680 Oceanogr. 36, 1–44.
681
682 Mahowald, N.M., 2007. Anthropocene changes in desert area: Sensitivity to climate model predictions.
683 Geophys. Res. Lett. 34, L18817.
684
685 Mahowald, N.M., Luo, C., 2003. A less dusty future? Geophys. Res. Lett. 20, 1903.
686
687 Mahowald, N., Baker, A.R., Bergametti, G., Brooks, N., Duce, R.A., Jickells, T.D., Kubilay, N., Prospero,
688 J.M., Tegen, I., 2005. Atmospheric global dust cycle and iron inputs to the ocean. Global Biogeochem.
689 Cycles 19, GB4025.
690
691 Mahowald, N.M., Muhs, D.R., Levis, S., Rasch, P.J., Yoshioka, M., Zender, C.S., Luo, C., 2009. Atmospheric
692 iron deposition: Global distribution, variability, and human perturbations. Annu. Rev. Mar. Sci. 1, 245–
693 278.
694
695 Massey, F.J., 1951. The Kolmogorov-Smirnov Test for Goodness of Fit. J. Amer. Statist. Assoc. 46, 68–78.
696
697 Measures, C.I., 1995. The distribution of Al in the IOC stations of the eastern Atlantic between 30°S and
698 34°N. Mar. Chem. 49, 267–281.
699
700 Measures, C.I., and Brown, E.T., 1996. Estimating dust input to the Atlantic Ocean using surface water Al
701 concentrations. *The Impact of Desert Dust Across the Mediterranean*, S. Guerzoni and R. Chester, Eds.,
702 Kluwer Acad., 301–311.
703
704 Measures, C.I., Edmond, J.M., 2000. Aluminium in the South Atlantic: steady state distribution of a short
705 residence time element. J. Geophys. Res. 95, 5331–5340.
706
707 Measures, C.I., Vink, S., 2000. On the use of dissolved aluminum in surface waters to estimate dust
708 deposition to the ocean. Global Biogeochem. Cycles 14, 317–327.
709
710 Measures, C.I., Landing, W.M., Brown, M.T., Buck, C.S., 2008a. High-resolution Al and Fe data from the
711 Atlantic Ocean CLIVAR-CO2 Repeat Hydrography A16N transect: Extensive linkages between
712 atmospheric dust and upper ocean geochemistry. Global Biogeochem. Cycles 22, GB1005, doi:
713 10.1029/2007GB003042.
714
715 Measures, C. I., Landing, W.M., Brown, M.T., Buck, C.S., 2008b. A commercially available rosette system
716 for trace metal-clean sampling. Limnol. Oceanogr. Methods 6, 384–394.
717
718 Measures, C., Hatta, M., Fitzsimmons, J., Morton, P., 2014. Dissolved Al in the zonal N Atlantic section of
719 the US GEOTRACES 2010/2011 cruises and the importance of Hydrothermal inputs. Deep-Sea
720 Res. II doi: 10.1016/j.dsr2.2014.07.006.

Mishchencko, M.I., Geogdzhayev, I.V., 2007. Satellite remote sensing reveals regional tropospheric aerosol trends. Opt. Exp. 15, 7423–7438.

Mishchenko, M.I., Geogdzhayev, I.V., Rossow, W.B., Cairns, B., Carlson, B.E., Lacis, A.A., Liu, L., Travis, L.D., 2007. Long-term satellite record reveals likely recent aerosol trend. Science 315, 1543.

Moran, S.B., Moore, R.M., 1988. Temporal variations in dissolved and particulate aluminum during a spring bloom. Estuar. Coast. Shelf Sci. 27, 205–215.

Moulin, C., Lambert, C.E., Dayan, U., Masson, V., Ramonet, M., Bousquet, P., Legrand, M., Balkanski, Y.J., Guelle, W., Marticorena, B., Bergametti, G., Dulac, F., 1998. Satellite climatology of African dust transport in the Mediterranean atmosphere. J. Geophys. Res. 103, 13137–13144.

Niedermeier, N., Held, A., Müller, T., Heinold, B., Schepanski, K., Tegen, I., Kandler, K., Ebert, M., Weinbruch, S., Read, K., Lee, J., Fomba, K.W., Müller, K., Herrmann, H., Wiedensohler, A., 2014. Mass deposition fluxes of Saharan mineral dust to the tropical northeast Atlantic Ocean: an intercomparison of methods. Atmos. Chem. Phys. 14, 2245–2266.

Ohnemus, D.C., Lam, P.J., 2014. Cycling of Lithogenic Marine Particles in the US GEOTRACES North Atlantic Transect. Deep-Sea Res. II, doi:10.1016/j.dsr2.2014.11.019.

Orians, K.J., Bruland, K.W., 1986. The biogeochemistry of aluminum in the Pacific Ocean. Earth Planet. Sci. Lett. 78, 397–410.

Pey, J., Querol, X., Alastuey, A., Forastiere, F., Stofoggia, M., 2013. African dust outbreaks over the Mediterranean Basin during 2011–2011: PM10 concentrations, phenomenology and trends, and its relation with synoptic and mesoscale meteorology. Atmos. Chem. Phys. 13, 1395–1410.

Planquette, H., Sherrell, R.M., 2012. Sampling for particulate trace metal determination using water sampling bottles: methodology to in situ pumps. Limnol. Oceanogr. Methods 10, 367–388.

Prospero, J.M., Lamb, P.J., 2003. African droughts and dust transport to the Caribbean: Climate change implications. Science 302, 1024–1027.

Prospero, J.M., Mayol-Bracero, O.L., 2013. Understanding the transport and impact of African dust on the Caribbean basin. Bull. Amer. Meteor. Soc. 94, 1329–1337.

Prospero, J.M., Landing, W.M., Schultz, M., 2010. African dust deposition to Florida: Temporal and spatial variability and comparisons to models. J. Geophys. Res. 115, D13304.

Resing, J.A., C.I. Measures, C.I., 1994. Fluorometric determination of Al in seawater by FIA with in-line preconcentration. Anal. Chem. 66, 4105–4111.

Ridame, C., Guieu, C., Löye-Pilot, M.-D., 1999. Trend in total atmospheric deposition fluxes of aluminium, iron, and trace metals in the northwestern Mediterranean over the past decade (1985–1997). J. Geophys. Res. 104, 30127–30138.

769 Ryder, C.L., Highwood, E.J., Rosenberg, P.D., Trembath, J., Brooke, J.K., Dean, A., Crosier, J., Dorsey, J.,
770 Brindley, H., Banks, J., Marsham, J.H., McQuaid, J.B., Sodemann, H., Washington, R., 2013. Optical
771 properties of Saharan dust aerosol and contribution form the coarse mode as measured during Fennec
772 2011 aircraft campaign. Atmos. Chem. Phys. 13, 303–325.
773
774 Schultz, M., Prospero, J.M., Baker, A.R., Dentener, F., Ickes, L., Liss, P.S., Mahowald, N.M., Nickovic, S,
775 García-Pando, C.P., Rodríguez, S., Sarin, M., Tegen, I., Duce, R.A., 2012. Atmospheric transport and
776 deposition of mineral dust to the ocean: Implications for research needs. Environ. Sci. Tech. 46, 10390–
777 10404.
778
779 Tegen, I., Werner, M., Harrison, S.P., Kohfeld, K.E., 2004. Relative importance of climate and land use in
780 determining present and future soil dust emission. Geophys. Res. Lett. 31, L05105.
781
782 Trossman, D.S., Thompson, L., Mecking, S., Warner, M.J., 2012. On the formation, ventilation, and
783 erosion of mode waters in the North Atlantic and Southern Oceans. J. Geophys. Res. 117, C09026.
784
785 Twining, B.S., Rauschenberg, S., Morton, P.L., Ohnemus, D.C., Lam, P.J., 2014. Comparison of particulate
786 trace element concentrations in the North Atlantic Ocean as determined with discrete bottle sampling
787 and in situ pumping. Deep-Sea Res. II, doi:10.1016/j.dsr2.2014.11.005.
788
789 Ussher, S.J., Achterberg, E.P., Powell, C., Baker, A.R., Jickells, T.D., Torres, R., Worsfold, P.J., 2013. Impact
790 of atmospheric deposition on the contrasting iron biogeochemistry of the North and South Atlantic
791 Ocean. Global Biogeochem. Cycles 27, 1096–1107.
792
793 van Hulten, M.M.P., Sterl, A., Tagliabue, A., Dutay, J.-C., Gehlen, M., de Baar, H.J.W., Middag, R., 2013.
794 Aluminum in an ocean general circulation model compared with the West Atlantic Geotraces cruise. J.
795 Mar. Sys. 126, 3–23.
796
797 Wedepohl, K.H., 2005. The composition of the continental crust. Geochim. Cosmochim. Acta 59, 1217–
798 1232.
799
800 Wong, S., Dessler, A.E., Mahowald, N.M., Colarco, P.R., da Silva, A., 2008. Long-term variability in
801 Saharan dust transport and its link to North Atlantic sea surface temperature. Geophys. Res. Lett. 35,
802 L07812.
803
804 Woodward, S., Roberts, D.L., Betts, R.A., 2005. A simulation of the effect of climate change-induced
805 desertification on mineral dust aerosol. Geophys. Res. Lett. 32, L18810.
806
807 Zender, C.S., Bian, H., Newman, D., 2003. Mineral Dust Entrainment and Deposition (DEAD) model:
808 description and dust climatology. J. Geophys. Res. 104, 4416.
809
810 Zhang, J., Reid, J.S., 2010. A decadal regional and global trend analysis of the aerosol optical depth using
811 a data assiilation grade over-water MODIS and Level 2 MISR aerosol products. Atmos. Chem. Phys. 10,
812 10949–10963.
813
814 Zhao, T.X.-P., Laszlo, I., Guo, W., Heidinger, A., Cao, A., Jelenak, A., Tarpley, D., Sullivan, J., 2008. Study of
815 long-term trend in aerosol optical thickness observed from operational AVHRR satellite instrument. J.
816 Geophys. Res. 113, D07201.

**Fig. 1**. Map of the CLIVAR/$CO_2$ Repeat Hydrography section A16N occupied in 2003 and 2013.

**Fig. 2**. Distributions of particulate Al (a-c) and particulate Fe (d-f) in nmol $L^{-1}$ along CLIVAR A16N in 2003 (a,d) and 2013 (b,e) with contours of potential density and the difference (2013 minus 2003) in particulate Al and Fe concentrations between the two occupations (c,f). Black dots represent individual sample measurements.

**Fig. 3**. Concentrations (in nmol $L^{-1}$) of particulate Al (diamonds, solid line) and particulate Si (circles, dotted line) at 45°N along CLIVAR A16N in 2003 (station 42, open symbols) and 2013 (station 41, closed symbols).

**Fig. 4**. Distributions of dissolved Al in nmol $L^{-1}$ along CLIVAR A16N in 2003 (a; Measures et al., 2008a) and 2013 (b; this work) with contours of potential density and the difference (2013 minus 2003) in dissolved Al concentrations between the two occupations (c). Black dots represent individual sample measurements.

**Fig. 5**. Difference (2013 minus 2003) in dissolved Al concentrations (in nmol $L^{-1}$) averaged over 25° to 35°N plotted as a function of potential density ($\sigma_\theta$).

**Fig. 6**. Maximum concentrations of dissolved Al (in nmol $L^{-1}$) in Mediterranean outflow water (MOW; 800–1300 m) from the 2013 CLIVAR A16N cruise (circles; this work), the 2010 GEOTRACES North Atlantic GA03 cruise (crosses; Measures et al., 2014), the 2002 IRONAGES III cruise (diamonds; Kramer et al., 2004), the 1998 MERLIM98 cruise (squares; de Jong et al., 2007), the 1990 IOC Atlantic cruise (triangles; Measures, 1995), and the 1982 RSS Discovery cruise 125 (inverted triangles; Hydes, 1983).

**Fig. 7**. Observed concentrations (in nmol $L^{-1}$) of pAl and pFe in subsurface particulate plume (0-20°N, >200 m), dAl in surface waters (>50m, 0-20°N), and dAl within the core of North Atlantic subtropical mode waters (25-35°N, 150–450m). Box plots show median values (solid line), 50$^{th}$ percentile values (box outline), 95$^{th}$ percentile values (whiskers), and outlier values (crosses).

**Fig. 8**. Aerosol optical depth at 550 nm from MODIS Terra Daily Level-3 Data temporally averaged over sampling dates (top) and 12 months prior to the cruise start (bottom) for the 2003 (left) and 2013 (right) occupations of A16N. Visualizations produced using the Giovanni online data system developed by NASA GES DISC (http://disc.sci.gsfc.nasa.gov/giovanni).

**Table 1**. Analysis (average ± 1 SD) of SAFe and GEOTRACES reference samples using the flow injection method of Resing and Measures (1994) for shipboard determination of dAl (nmol $L^{-1}$) during the 2013 occupation of A16N compared to consensus values as of May 2013 (http://www.geotraces.org/science/intercalibration).

| | | A16N 2013 | consensus |
|---|---|---|---|
| SAFe S | (n=8) | 1.83 ± 0.05 | 1.67 ± 0.10 |
| SAFe D1 | (n=8) | 1.01 ± 0.02 | 0.62 ± 0.03 |
| SAFe D2 | (n=8) | 0.93 ± 0.04 | 1.03 ± 0.09 |
| GEO GD | (n=7) | 17.5 ± 0.4 | 17.7 ± 0.2 |
| GEO GS | (n=4) | 29.6 ± 1.3 | 27.5 ± 0.2 |

**Table 2**. Observed changes in trace metal concentrations between 2003 and 2013 reported in nmol $L^{-1}$ and % change since 2003 and estimated residence time of the trace metal signal in regions of high aerosol dust inputs along A16N.

| trace metal feature | latitude range | depth range | residence time | avg change 2003–2013 in nmol $L^{-1}$ (%) |
|---|---|---|---|---|
| equatorial subsurface particulate Al | 0–20°N | > 200 m | 1–4 years | 1.6 (+14%) |
| equatorial subsurface particulate Fe | 0–20°N | > 200 m | 1–4 years | 0.9 (+27%) |
| equatorial surface dissolved Al | 0–20°N | < 50 m | months | 3.1 (+16%) |
| NA STMW[a] dissolved Al | 25–35°N | 150–450 m | 4–20 years | 1.0 (+5%) |

[a]North Atlantic subtropical mode water

Figure 1

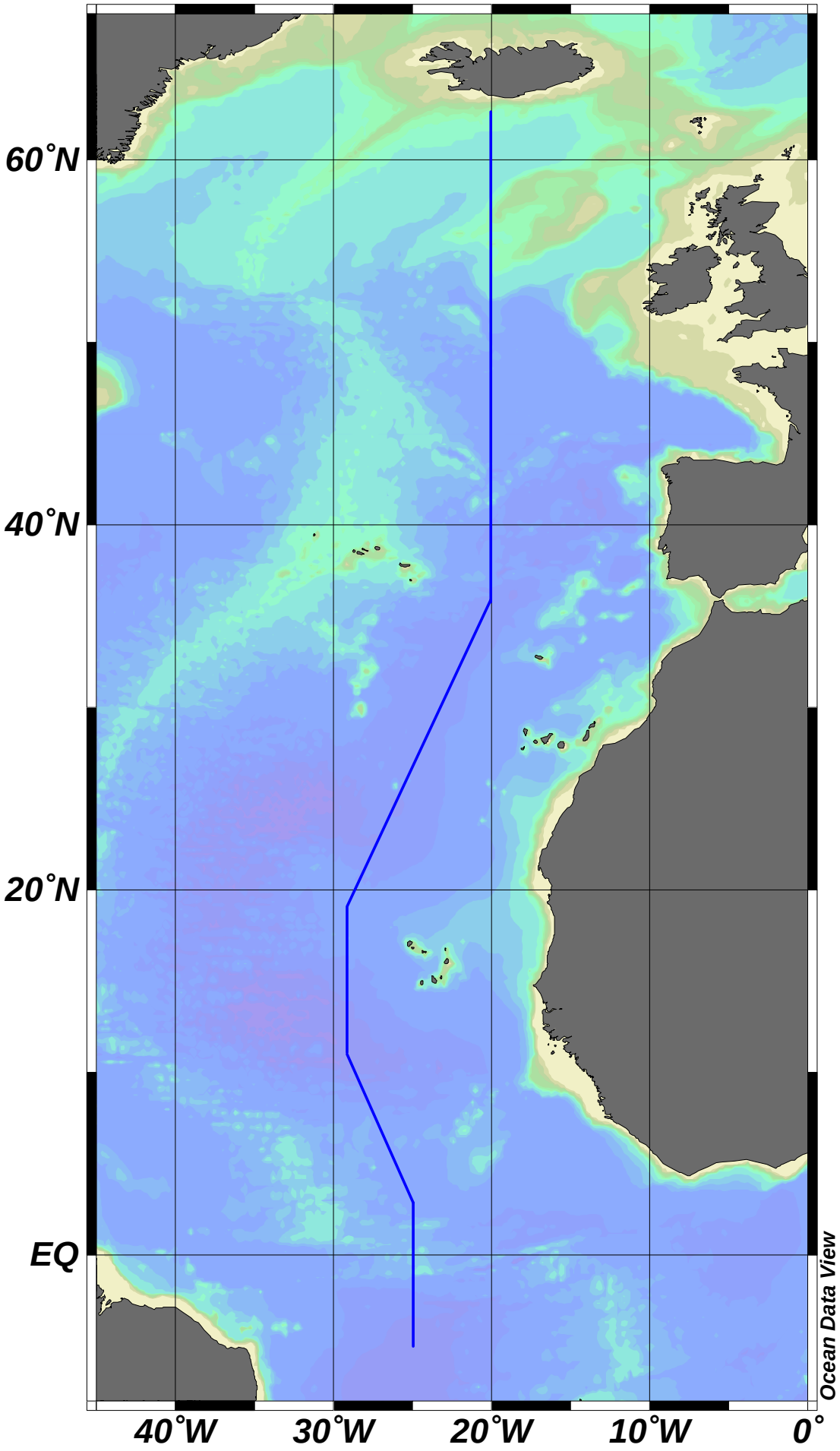

**Figure 2**

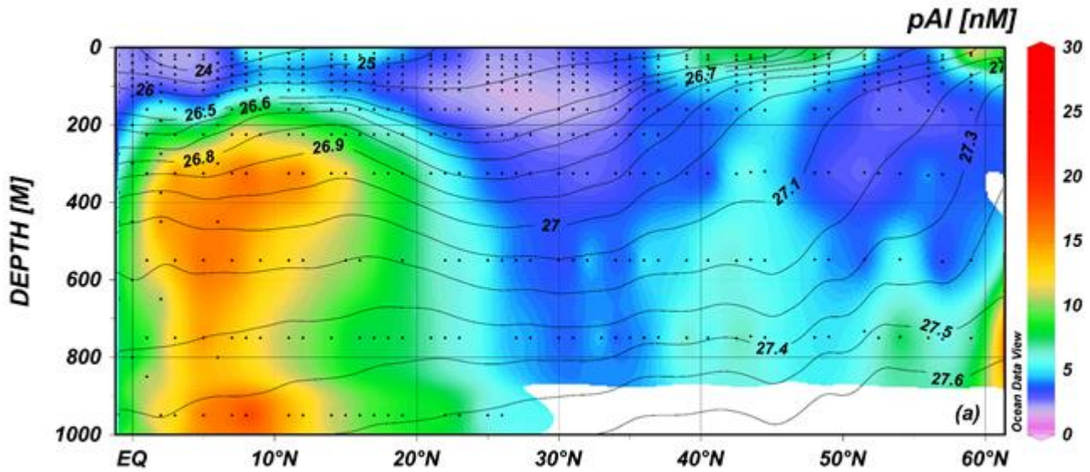
pAl [nM]
DEPTH [M]
0
200
400
600
800
1000
EQ
10°N
20°N
30°N
40°N
50°N
60°N
24
25
26
26.5
26.6
26.7
26.8
26.9
27
27.1
27.3
27.4
27.5
27.6
30
25
20
15
10
5
0
Ocean Data View
(a)

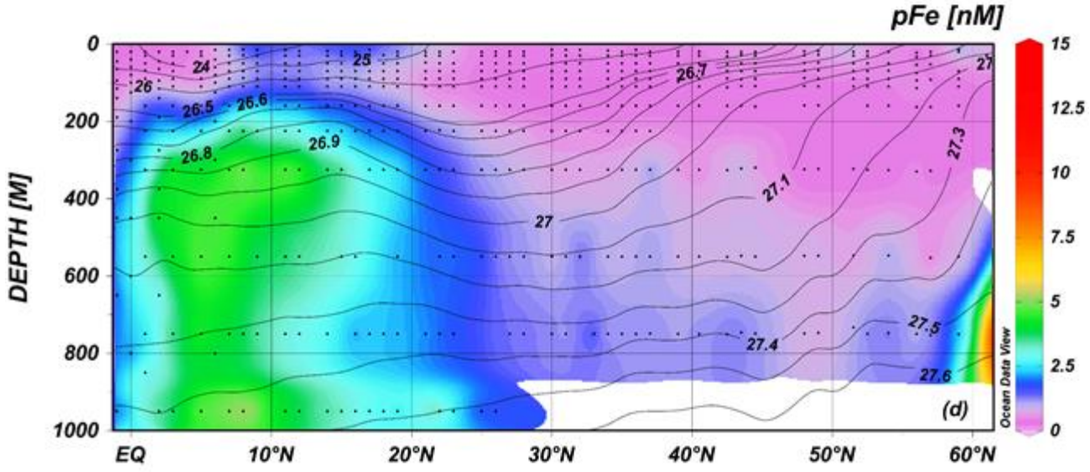
pFe [nM]
DEPTH [M]
0
200
400
600
800
1000
EQ
10°N
20°N
30°N
40°N
50°N
60°N
24
25
26
26.5
26.6
26.7
26.8
26.9
27
27.1
27.3
27.4
27.5
27.6
15
12.5
10
7.5
5
2.5
0
Ocean Data View
(d)

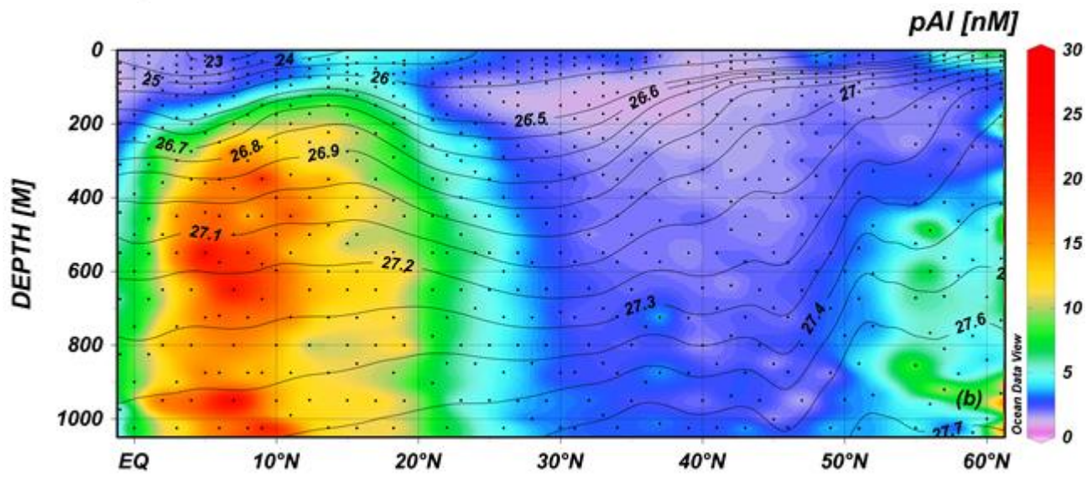
pAl [nM]
DEPTH [M]
0
200
400
600
800
1000
EQ
10°N
20°N
30°N
40°N
50°N
60°N
23
24
25
26
26.5
26.6
26.7
26.8
26.9
27
27.1
27.2
27.3
27.4
27.6
30
25
20
15
10
5
0
Ocean Data View
(b)

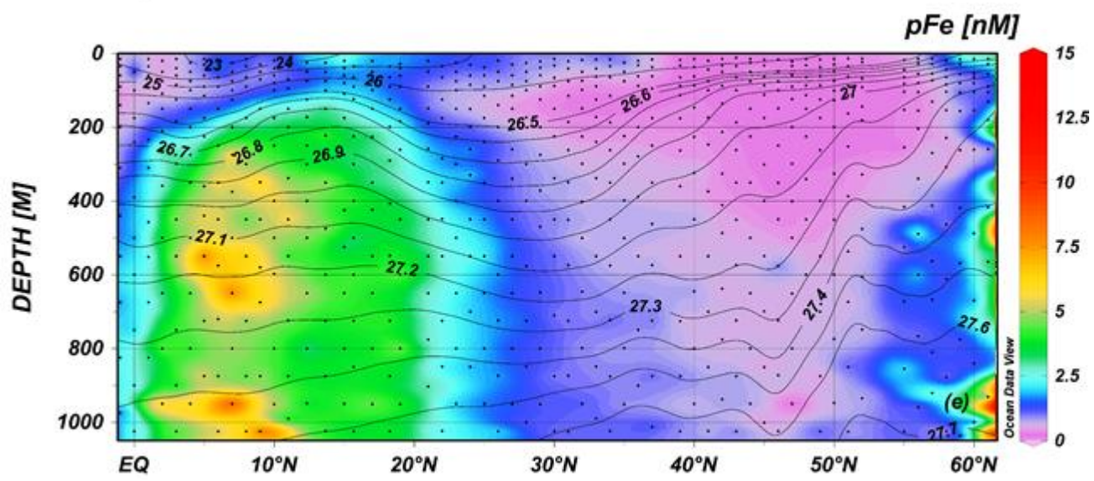
pFe [nM]
DEPTH [M]
0
200
400
600
800
1000
EQ
10°N
20°N
30°N
40°N
50°N
60°N
23
24
25
26
26.5
26.6
26.7
26.8
26.9
27
27.1
27.2
27.3
27.4
27.6
15
12.5
10
7.5
5
2.5
0
Ocean Data View
(e)

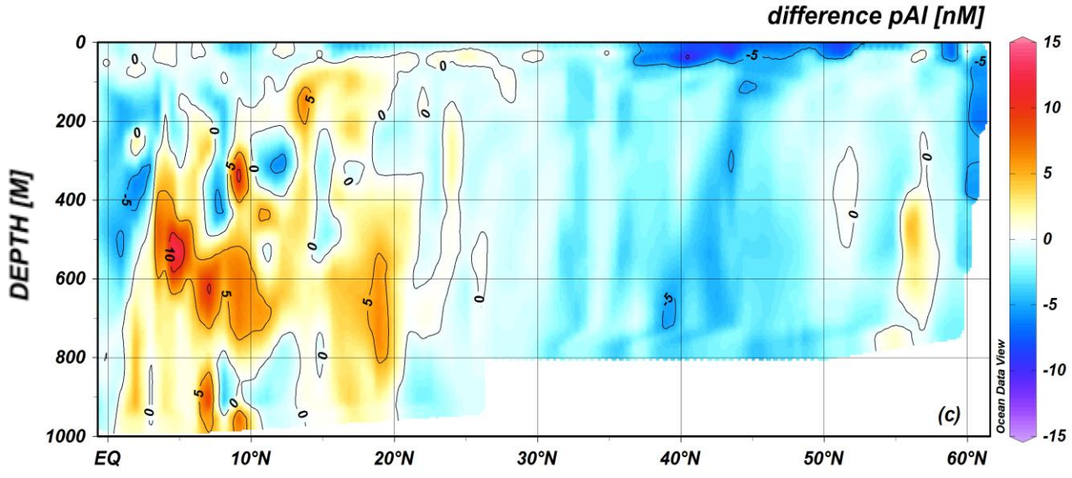
difference pAl [nM]
DEPTH [M]
0
200
400
600
800
1000
EQ
10°N
20°N
30°N
40°N
50°N
60°N
15
10
5
0
-5
-10
-15
Ocean Data View
(c)

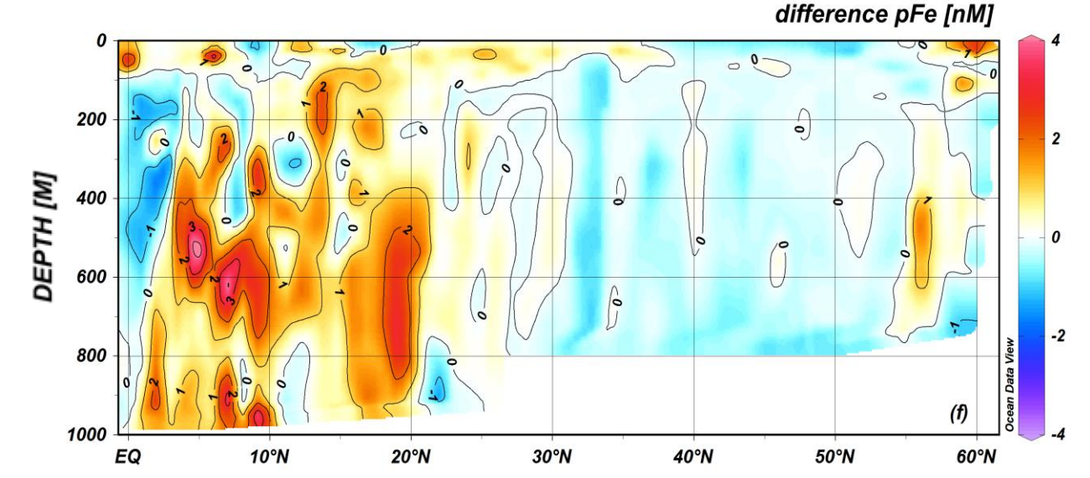
difference pFe [nM]
DEPTH [M]
0
200
400
600
800
1000
EQ
10°N
20°N
30°N
40°N
50°N
60°N
4
2
0
-2
-4
Ocean Data View
(f)

**Figure 3**

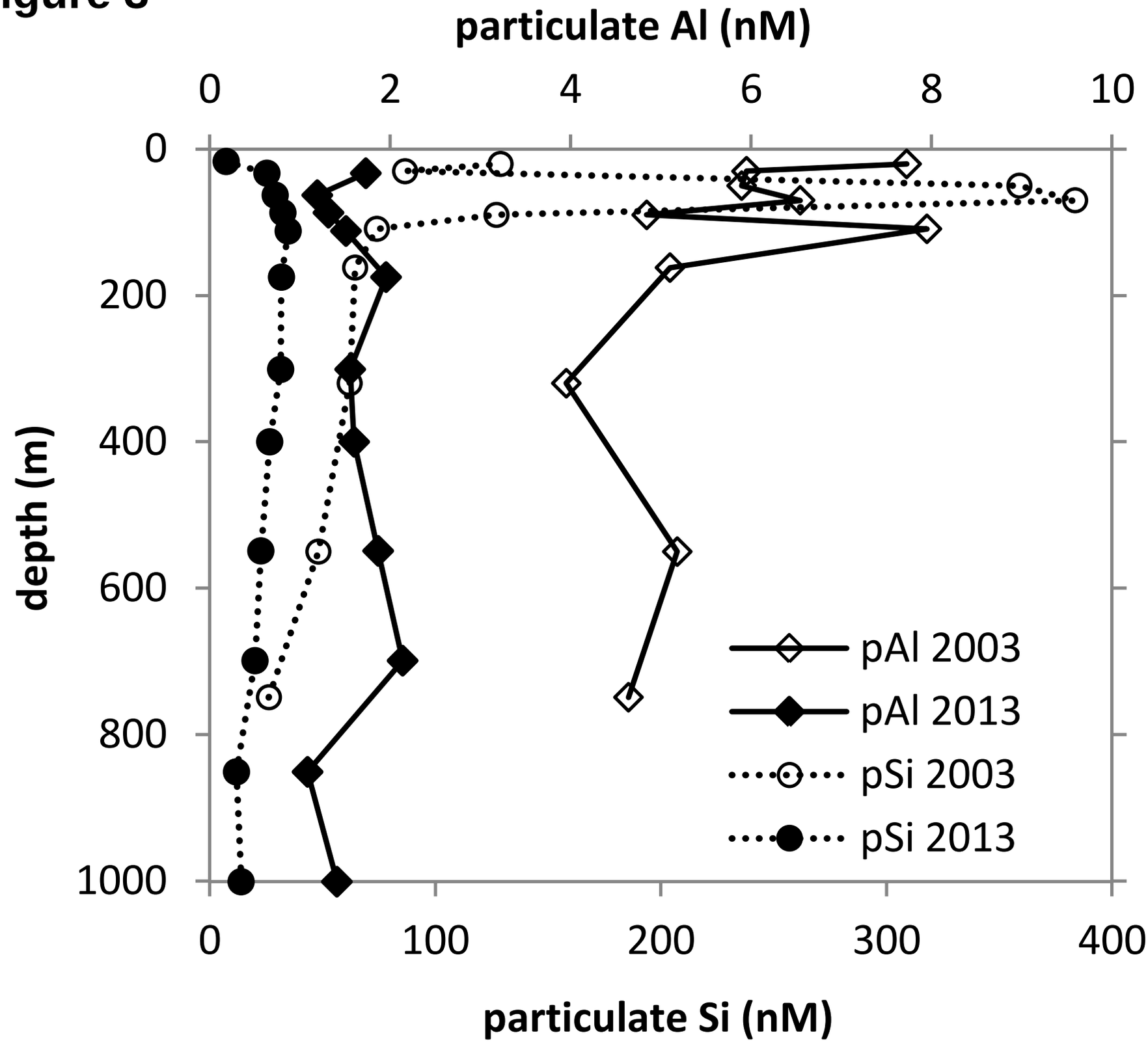
particulate Al (nM)
0
2
4
6
8
10
depth (m)
0
200
400
600
800
1000
pAl 2003
pAl 2013
pSi 2003
pSi 2013
0
100
200
300
400
particulate Si (nM)

Figure 4

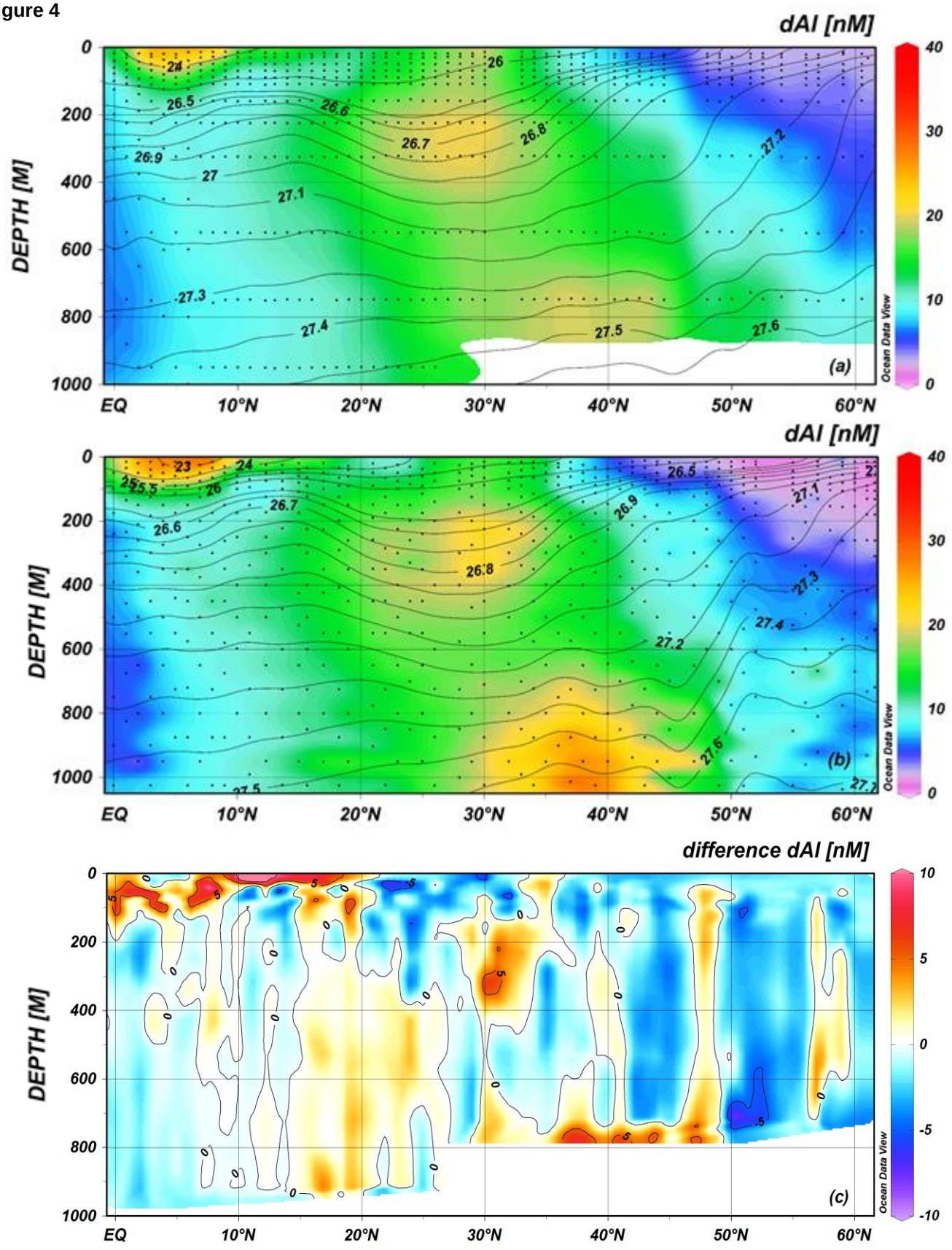
dAl [nM]
DEPTH [M]
0
200
400
600
800
1000
EQ
10°N
20°N
30°N
40°N
50°N
60°N
24
26
26.5
26.6
26.7
26.8
26.9
27
27.1
27.2
27.3
27.4
27.5
27.6
(a)
40
30
20
10
0
Ocean Data View
dAl [nM]
23
24
25.5
26
26.5
26.6
26.7
26.8
26.9
27.1
27.2
27.3
27.4
27.5
27.6
(b)
difference dAl [nM]
10
5
0
-5
-10
(c)

**Figure 5**

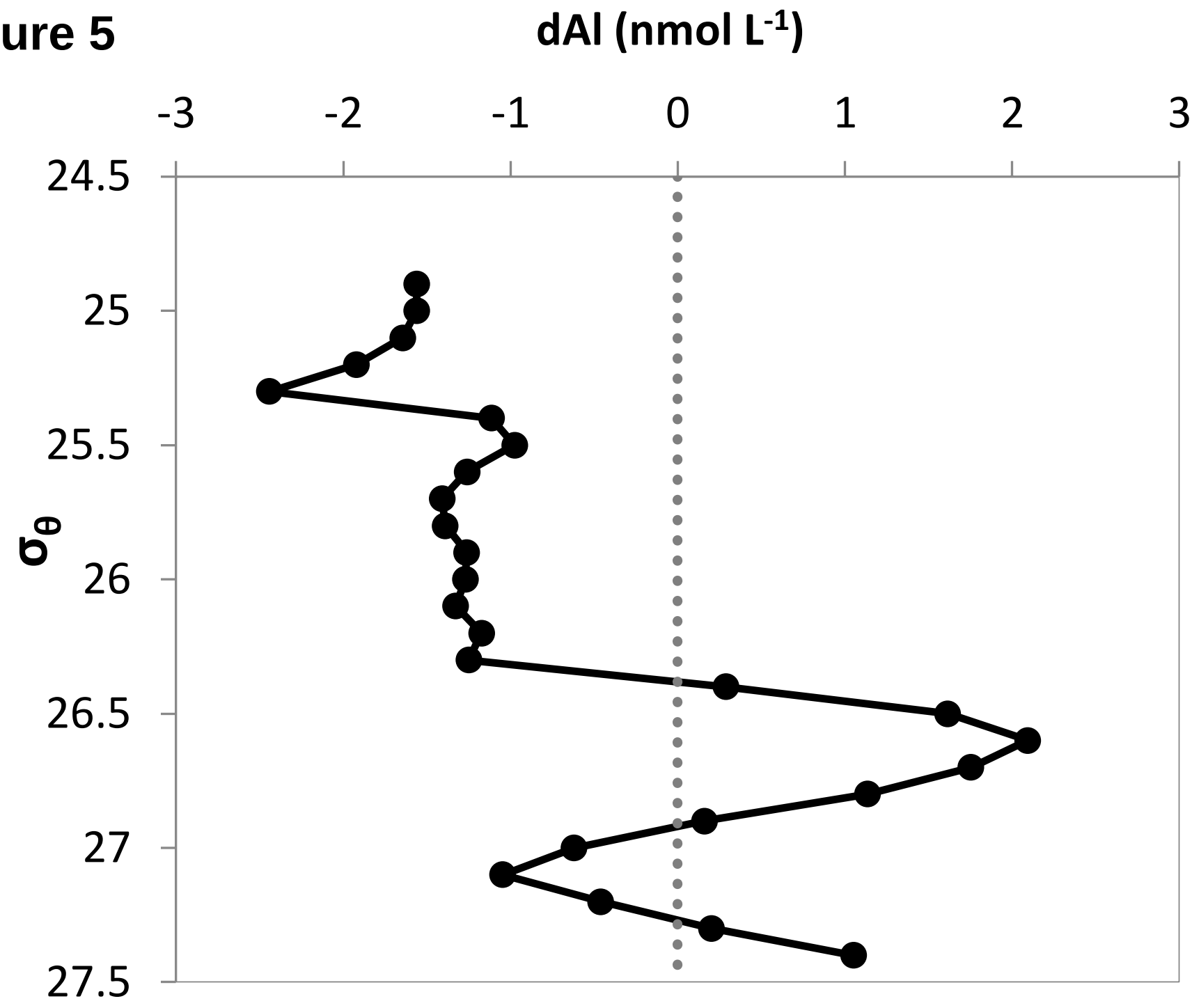

Figure 6

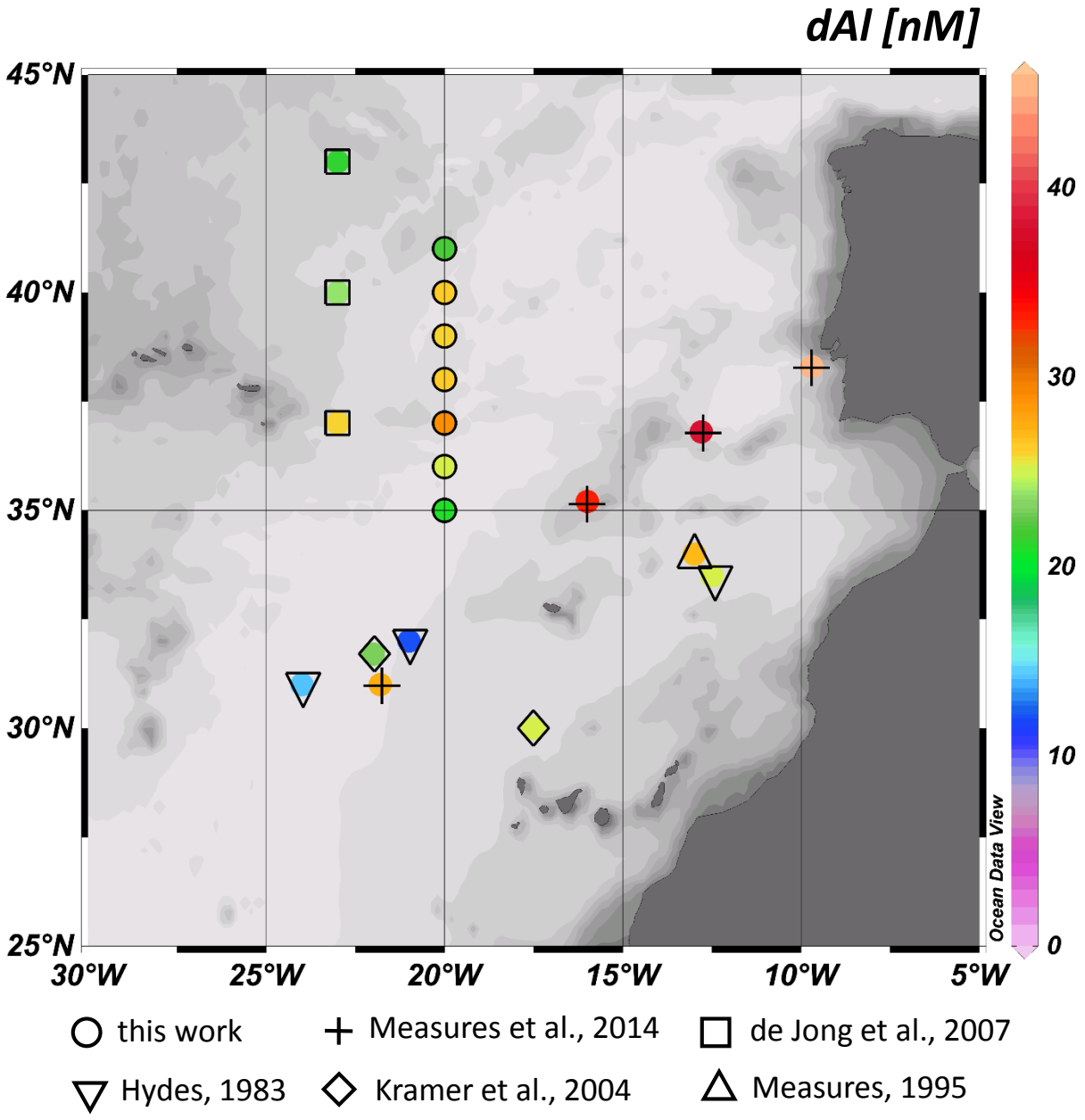
dAl [nM]
45°N
40°N
35°N
30°N
25°N
30°W
25°W
20°W
15°W
10°W
5°W
40
30
20
10
0
Ocean Data View
this work
Measures et al., 2014
de Jong et al., 2007
Hydes, 1983
Kramer et al., 2004
Measures, 1995

Figure 7

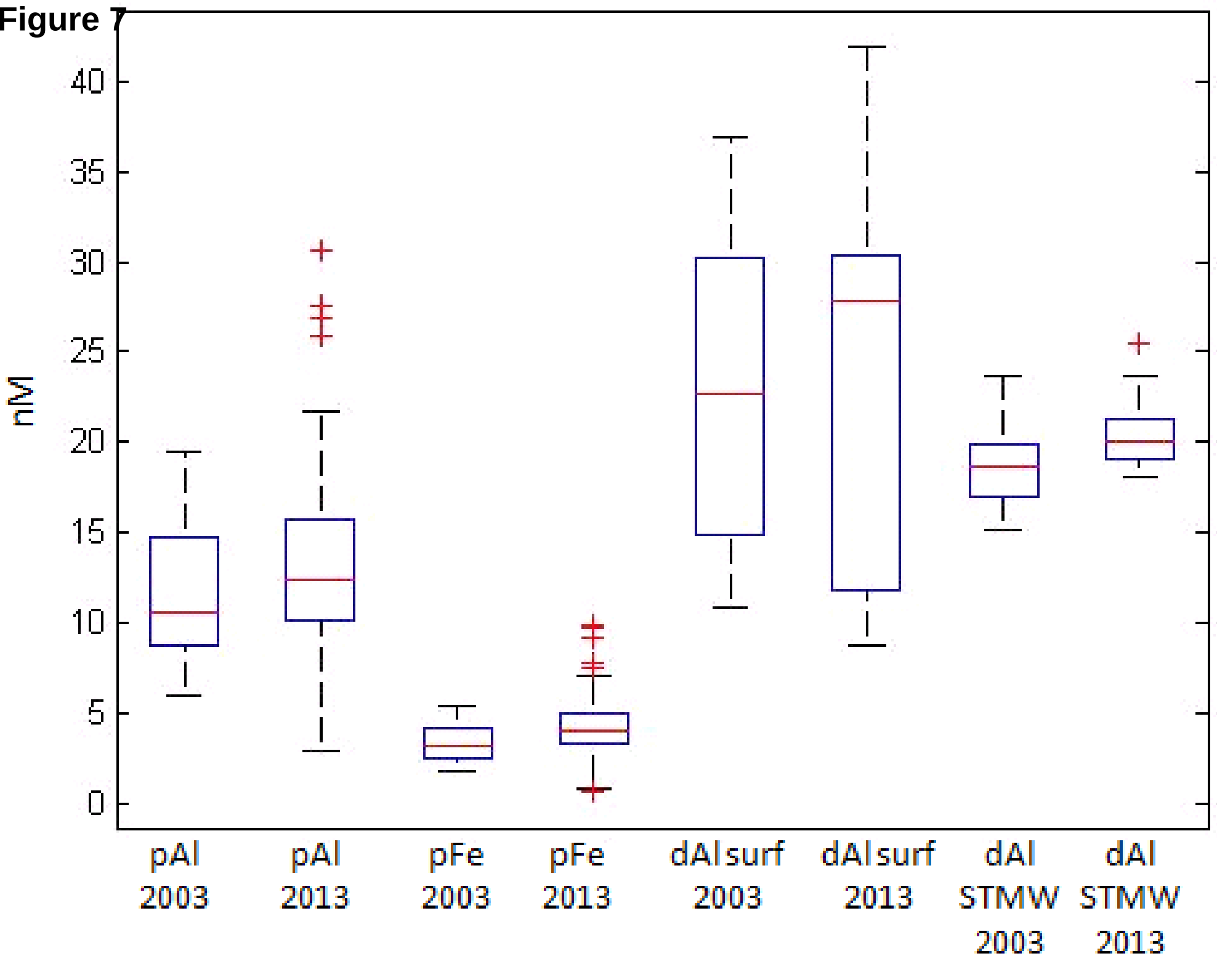
nM
0
5
10
15
20
25
30
35
40
pAl 2003
pAl 2013
pFe 2003
pFe 2013
dAlsurf 2003
dAlsurf 2013
dAl STMW 2003
dAl STMW 2013

Figure 8

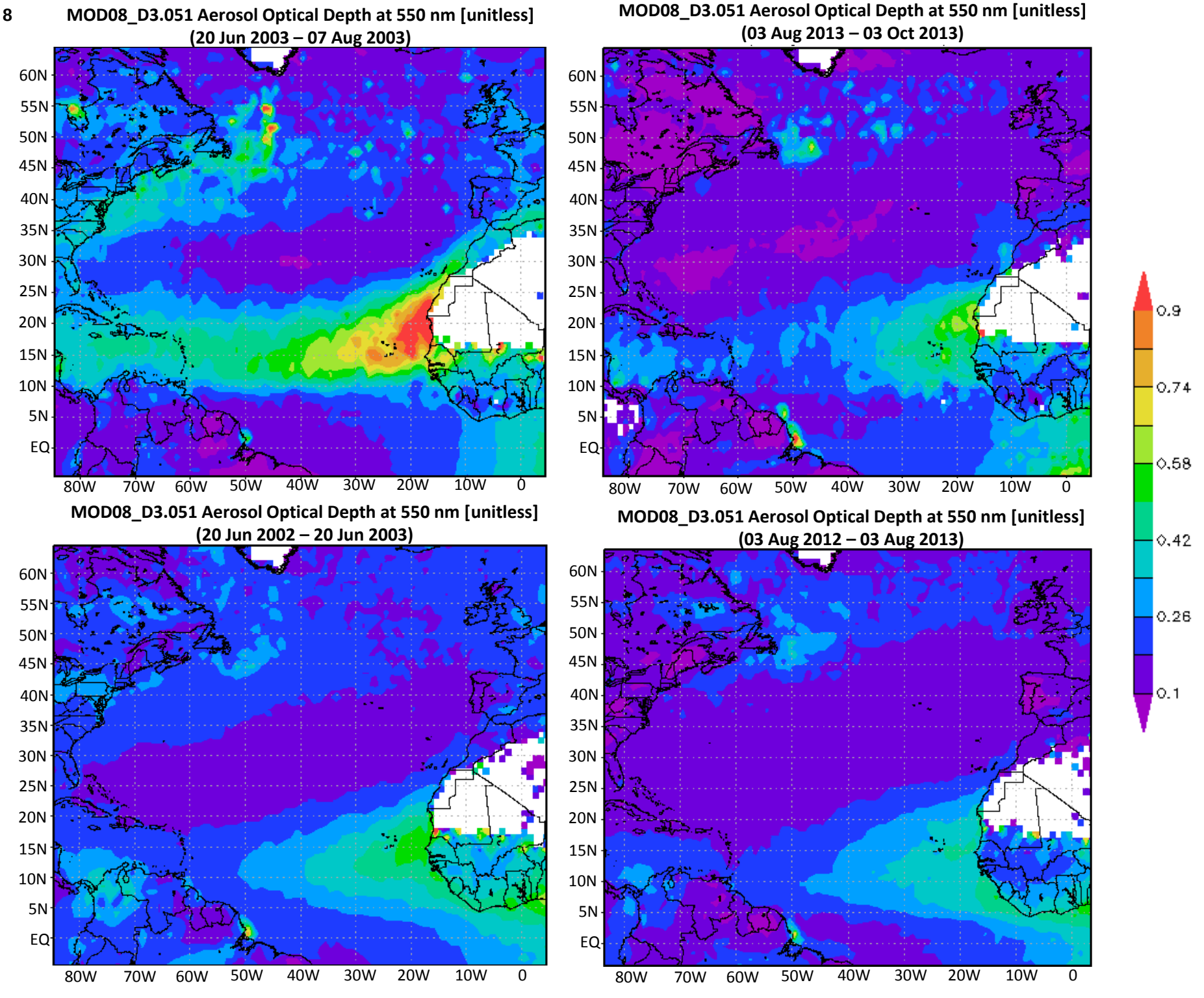
MOD08_D3.051 Aerosol Optical Depth at 550 nm [unitless]
(20 Jun 2003 – 07 Aug 2003)
MOD08_D3.051 Aerosol Optical Depth at 550 nm [unitless]
(03 Aug 2013 – 03 Oct 2013)
MOD08_D3.051 Aerosol Optical Depth at 550 nm [unitless]
(20 Jun 2002 – 20 Jun 2003)
MOD08_D3.051 Aerosol Optical Depth at 550 nm [unitless]
(03 Aug 2012 – 03 Aug 2013)
60N
55N
50N
45N
40N
35N
30N
25N
20N
15N
10N
5N
EQ
80W
70W
60W
50W
40W
30W
20W
10W
0
0.9
0.74
0.58
0.42
0.26
0.1